Biomech Model Mechanobiol
DOI 10.1007/s10237-009-0187-9

ORIGINAL PAPER

Stress-dependent morphogenesis: continuum mechanics and truss systems

José J. Muñoz · Vito Conte · Mark Miodownik

Received: 20 July 2009 / Accepted: 22 December 2009

Abstract A set of equilibrium equations is derived for the stress-controlled shape change of cells due to the remodelling and growth of their internal architecture. The approach involves the decomposition of the deformation gradient into an active and a passive component; the former is allowed to include a growth process, while the latter is assumed to be hyperelastic and mass-preserving. The two components are coupled with a control function that provides the required feedback mechanism. The balance equations for general continua are derived and, using a variational approach, we deduce the equilibrium equations and study the effects of the control function on these equations. The results are applied to a truss system whose function is to simulate the cytoskeletal network constituted by myosin microfilaments and microtubules, which are found experimentally to control shape change in cells. Special attention is paid to the conditions that a thermodynamically consistent formulation should satisfy. The model is used to simulate the multicellular shape changes observed during ventral furrow invagination of the *Drosophila melanogaster* embryo. The results confirm that ventral furrow invagination can be achieved through stress control alone, without the need for other regulatory or signalling mechanisms. The model also reveals that the yolk plays a distinct role in the process, which is different to its role during invagination with externally imposed strains. In stress control, the incompressibility constraint of the yolk leads, via feedback, to the generation of a pressure in the ventral zone of the epithelium that eventually eases its rise and internalisation.

Keywords Morphogenesis · Trusses · Embryo · Development · Feedback

J. J. Muñoz (✉)
Laboratori de Càlcul Numèric (LaCàN),
Department of Applied Mathematics III, Universitat Polit. Catalunya, Barcelona, Spain
e-mail: j.munoz@upc.edu

V. Conte · M. Miodownik
Materials Research Group, Division of Engineering,
King's College London, London, UK

1 Introduction

In accordance with the common terminology employed in biomechanics (Taber 1995), the changes in biomechanical processes may be classified as growth (change of mass), remodelling (change of density or other material properties such as fibre orientation) or morphogenesis (change of shape). In this article, we apply these basic principles to model the reorganisation process of the structural elements in the cytoskeleton of epithelial cells during ventral furrow invagination (first morphogenetic movement taking place in the embryo development of *Drosophila Melanogaster*).

We first split the global deformation of a cell into an active part that represents the mechanotransduction of the chemical bonds in the cytoskeleton, induced by the gene expression, and a passive part that corresponds to the assumed elastic response. In the active component, we assume that the density remains constant, although mass may be added or removed from the system (growth); this process, when applied to a unidimensional bar, physically corresponds to the elongation or shortening of microtubules and microfilaments. Such local length changes produce a passive reorientation of these elements (remodelling) and a subsequent global shape change (morphogenesis) of the epithelial cells. Therefore, by modelling a local growth process, we reproduce a remodelling of the epithelial cells, and in turn global morphogenesis in embryo development. It is not our aim to analyse the source

Published online: 13 January 2010

of the cytoskeleton reorganisation, which is a wide debated topic (see for instance Mizuno et al. 2007).

The constitutive law employed for the growth and remodelling processes has been formalised in different ways depending on the physical phenomena being modelled (Ambrosi and Guana 2007; Himpel et al. 2005; Kuhl and Steinmann 2004; Lubarda and Hoger 2002; Lubarda 2004; Rajagopal and Srinivasa 2004). In some of these approaches, the evolution laws of the active deformation are derived from the dependence of the internal energy on variables involved in the elastic process, such as the second Piola–Kirchhoff (Lubarda and Hoger 2002) or the Kirchhoff stresses (Himpel et al. 2005). Other authors deduce a form of the intermediate deformation by maximising the mechanical dissipation (Rajagopal and Srinivasa 2004). Alternatively, in Ambrosi and Guana (2007) and DiCarlo and Quiligotti (2002), the growth rate is induced by accretive forces, which equilibrate the externally supplied forces. In most of these cases, though, the evolution laws of the active component are such that the growth rate of the accretive stresses tend to achieve a stable (homeostatic) value, at which no further active deformation occurs. A similar idea can be found in Rodriguez et al. (1994), or more recently in Ramasubramanian and Taber (2008) and Taber (2008), based on Beloussov's hyper-restoration hypothesis (Beloussov et al. 1994; Beloussov 1998). This hypothesis states that whenever a local change in the elastic stresses is detected, the tissue tends to deform in order to restore the initial stress state, but as a rule overshooting it. This stress state may be attained at a constant (Ramasubramanian and Taber 2008) or a variable (Taber 2008) target stress.

In our case, the constitutive laws of the growth process are a function of the elastic stresses, in a similar manner to other models for blood vessels (Rodriguez et al. 1994; Humphrey 2001; Taber 1998), or for morphogenesis (Ambrosi and Guana 2007; Taber 2008). The former are based on experimental results, where it is observed that the tissues tend to a homeostatic state at which no further growth/resorption occurs. We here assume that this situation is reached when the stresses achieve a target stress, similar to Beloussov's hyper-restoration hypotheses. The particular form of the stress-controlled law has been motivated in our case by the stress profiles obtained in our earlier models where the active kinematic response of the cells was imposed externally (Muñoz et al. 2007; Conte et al. 2008).

On the other hand, the nonlinear elastic behaviour of adaptive isotropic chain networks have been studied in Boyce and Arruda (2000), Miehe et al. (2004), and the modelling of oriented chains, commonly found in biology, can be found in Kuhl et al. (2005, 2006). In the latter references, the forces produced by a network chain embedded in a cell arise due to the particular form of the Helmholtz free energy associated to the chain. In our case, we neglect any interaction between the actin–myosin chains, other than their connectivity at the chain ends. In addition, we assume that the active deformation preserves density but with a local mass increase due to the insertion in the system of new actin material, which in turn increases the elastic energy of the system.

Our model is formulated in the general context of continua, which, in order to apply the theory to modelling cytoskeletal filaments, is particularised and detailed for a truss system. Similar truss representations have been originally employed by Odell et al. (1981), which used a bistable mechanism in order to trigger invagination. In our model, the invagination is alternatively produced due to the specific stress-dependent growth law.

We note that biological structures have been also explicitly represented by resorting to tensegrity concepts, and although this approach has been fruitful in the modelling of self-equilibrated systems (Ingber 1997; Stamenović and Ingber 2009), its application to morphogenesis in conjunction with growth is absent in the literature. Although our approach shares some similarities with a tensegrity structure, we do not consider pre-stress, and we do not assume any *a priori* knowledge of the bars that will be in tension (cables) or in compression (rods).

The paper is organised as follows. Section 2 introduces some well-known facts about the kinematics and balance equations in continuum mechanics. This section also describes the fundamental laws of thermodynamics in the presence of active and passive (elastic) deformations. We deduce, in a variational approach, the equilibrium equations when the two components of the deformation are independent or dependent. Section 3 uses the same steps to obtain the equilibrium equations for a system of trusses. Section 4 compares the current approach to the standard elastic equations for a single active cell, and the truss theory is eventually applied to model the multicellular phenomenon of ventral furrow invagination of the *Drosophila melanogaster* embryo for which the involvement of active shape changes is thought to be pivotal. Section 5 comments on these results and expands on the work with some final remarks.

2 Development of continuum theory

2.1 Kinematics

We analyse in this section the deformation of a body $\mathcal{B}$ with *reference configuration* $\Omega^0 \in \mathbb{R}^3$ and material coordinates $\boldsymbol{X}^0$ into a *deformed configuration* $\Omega_t \in \mathbb{R}^3$ where the material points are located at $\boldsymbol{x} = \chi(\boldsymbol{X}^0, t)$, with $\chi(\boldsymbol{X}^0, t) : \mathbb{R}^3 \times \mathbb{R} \to \mathbb{R}^3$ the map of the whole motion. For clarity, we remove the dependence on the time variable t and the position $\boldsymbol{X}^0$, and simply denote by $\boldsymbol{x}$ the map χ. The notation

employed here and throughout the article has been listed in Table 1.

As it is customary in biomechanics since the seminal work of Rodriguez et al. (1994), we use a multiplicative decomposition of the deformation gradient $\boldsymbol{F} = \frac{\partial \boldsymbol{x}}{\partial \boldsymbol{X}^0}$ into $\boldsymbol{F} = \boldsymbol{F}_e \boldsymbol{F}_a$ (see Fig. 1). In the present case, the active deformation gradient $\boldsymbol{F}_a = \frac{\partial \boldsymbol{X}}{\partial \boldsymbol{X}^0}$ is due to the growth process in the cell, which in turn is due to the mechanotransduction of the genetically regulated chemical reactions that take place in the cytoskeleton. On the other hand, the tensor $\boldsymbol{F}_e = \frac{\partial \boldsymbol{x}}{\partial \boldsymbol{X}}$ represents the passive elastic deformation due to the elastic response of either the cytoskeleton and the cytoplasm. The intermediate configuration Ω is the one obtained after removing the elastic deformation from Ω_t, which may give rise to material incompatibilities (tears and overlappings, see Fig. 1). Therefore, the two tensors $\boldsymbol{F}_a$ and $\boldsymbol{F}_e$ may be discontinuous, while $\boldsymbol{F}$ is continuous. From the decomposition of the deformation gradient, and setting $J = det\,\boldsymbol{F}$, $J_a = det\,\boldsymbol{F}_a$ and $J_e = det\,\boldsymbol{F}_e$, we have that $J = J_a J_e$.

We denote by ρ^0, ρ and ρ_t the densities in the reference, intermediate and deformed configurations, respectively. Analogously, we denote by $(\mathrm{d}M^0, \mathrm{dV}^0)$, $(\mathrm{d}M, \mathrm{dV})$ and $(\mathrm{d}m, \mathrm{dv})$ the pairs of differentials of mass and volume in the same configurations (see Fig. 1), which are related by $\mathrm{d}M^0 = \rho^0 \mathrm{dV}^0$, $\mathrm{d}M = \rho \mathrm{dV}$ and $\mathrm{d}m = \rho_t \mathrm{dv}$.

2.2 Balance equations

2.2.1 Balance of mass

Throughout the paper, we use the following assumptions:

- The active deformations do not introduce any change of density, (i.e. $\rho = \rho^0, \forall t$), although changes of mass (growth) may occur when passing from configuration Ω^0 to Ω, (i.e. $\rho^0 \mathrm{dV}^0 \neq \rho \mathrm{dV}$ in general).
- The elastic deformation may introduce density changes when passing from the configuration Ω to Ω_t, (i.e. $\rho \neq \rho_t$ in general), although this transformation preserves the mass, (i.e. $\mathrm{d}M = \mathrm{d}m, \forall t$).

These assumptions are motivated by the model of the actin–myosin complex described in Sect. 3. We note that due to the non-conservation of mass, we are dealing with an open system as described in Kuhl and Steinmann (2003), but in our case with a constant reference density ρ^0. From the conditions $\mathrm{d}M = \mathrm{d}m$ and $\rho = \rho^0$, and the relation $\mathrm{dv} = J_e \mathrm{dV}$, it can be deduced that $\rho^0 = \rho_t J_e$, and therefore,

$$\dot{\overline{\rho_t J_e}} = \dot{\rho}^0 = 0, \tag{1}$$

where a superimposed dot denotes material time differentiation, i.e. $\dot{\square} = \dot{\overline{\square}} = \frac{\partial}{\partial t}|_{\boldsymbol{X}^0 = cnst}(\square)$. After making use of (1)

Table 1 Nomenclature and list of symbols employed in the article

A^0, a	Reference and deformed cross-sections of the bar
$\bar{\boldsymbol{b}}^0, \bar{\boldsymbol{b}}$	Body load per unit of reference and deformed volume, respectively
$C, \boldsymbol{C}$	Control function for the scalar and tensorial cases
$\mathcal{D}$	Dissipated energy
E	Total internal energy
$\boldsymbol{E}_i$	Triad vectors in the reference and intermediate configurations
$\boldsymbol{e}_i$	Triad vectors in the deformed configuration
$\boldsymbol{F}, \boldsymbol{F}_a, \boldsymbol{F}_e$	Total, active and elastic deformation gradients
G	Variable defined in Eq. (50)
$\boldsymbol{g}, \bar{\boldsymbol{g}}$	Internal and external contributions to bar residual
h_{ext}, h_{int}	External contribution (heating) and internal contribution to entropy
$\boldsymbol{I}, \boldsymbol{\mathcal{I}}$	Second and fourth-order identity tensors
J, J_a, J_e	Determinant of $\boldsymbol{F}$, $\boldsymbol{F}_a$ and $\boldsymbol{F}_e$, respectively
K	Total kinetic energy
$k, \boldsymbol{K}$	Bar material stiffness and stiffness matrix
L^0, L, ℓ	Bar lengths at the reference, intermediate and deformed configuration
$\boldsymbol{L}_a$	Active velocity gradient
$\boldsymbol{N}^0, \boldsymbol{N}, \boldsymbol{n}$	External normals in the reference, intermediate and deformed configuration
$\boldsymbol{L}_a$	Active velocity gradient
$\boldsymbol{p}$	Vector of linear momentum
$\boldsymbol{P}$	First Piola–Kirchhoff stress tensor
$\boldsymbol{Q}^0, \boldsymbol{Q}$	Thermal fluxes per unit of reference and deformed area
$\boldsymbol{q}, \bar{\boldsymbol{q}}$	Stress resultant and external load in bars
q_T	Target stress in the bar control function C
$\boldsymbol{R}$	Rotation matrix such that $\boldsymbol{e}_i = \boldsymbol{R}\boldsymbol{E}_i$
$S, \bar{S}$	Entropy density, and additional entropy source (due to new mass in the system)
$t, \Delta t$	Time variable, and time increment, $\Delta t = t_{n+1} - t_n$
$\bar{\boldsymbol{t}}^0, \bar{\boldsymbol{t}}$	Surface loads per unit of reference and deformed area
$\boldsymbol{u}, \boldsymbol{u}_a, \boldsymbol{u}_e$	Total, active and elastic displacement vectors
V^0, V, v	Volume in the reference, intermediate and deformed configuration
$\boldsymbol{v}$	Velocity vector, $\boldsymbol{v} = \dot{\boldsymbol{x}}$
$\boldsymbol{w}$	Test function in the weak form of the bar equil. eqn.
$\boldsymbol{X}^0, \boldsymbol{X}, \boldsymbol{x}$	Position vector of the material points in the reference, intermediate and deformed configuration
β	Constant in bar control function C
$\delta(\bullet)$	Variation operator, $\delta = \frac{d}{d\epsilon}\big\|_{\epsilon=0}$
Γ	Mass production rate
$\gamma, \gamma_a, \gamma_e$	Total, active and elastic scalar strain measures in bars
Π	Total energy functional
ψ^0	Helmholtz free energy function per unit of mass

Table 1 continued

ϕ^0, ϕ_t	Internal energy per unit of mass in the reference and deformed configuration, respectively
ε_{ijk}	Permutation index
$\boldsymbol{\varepsilon}$	Vectorial strain measure for bar element
ρ^0, ρ, ρ_t	Densities in the reference, intermediate and deformed configuration
$\Omega^0, \Omega, \Omega_t$	Domains of the body in the reference, intermediate and deformed configuration
$\boldsymbol{\sigma}$	Cauchy stress tensor
τ	Constant defined in Eq. (49)
θ	Parameter in Crank–Nicholson time-integration
Θ	Temperature

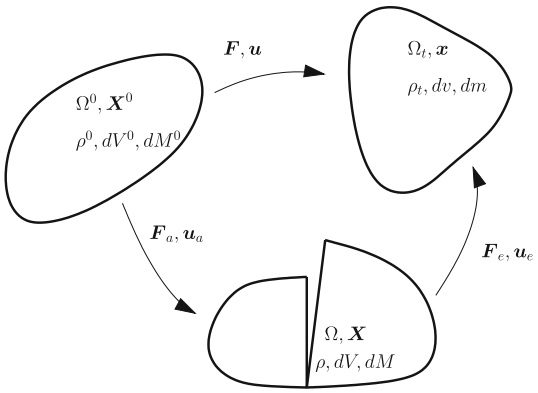

Fig. 1 Decomposition of the deformation gradient as $\boldsymbol{F} = \boldsymbol{F}_a \boldsymbol{F}_e$. The reference, intermediate and deformed configurations are indicated by Ω^0, Ω and Ω_t, respectively. Other variables associated to each configuration and map are indicated in the figure and described in the text

and the relation $\dot{J}_a = J_a \mathrm{tr}\boldsymbol{L}_a$, with $\boldsymbol{L}_a = \dot{\boldsymbol{F}}_a \boldsymbol{F}_a^{-1}$ the *active velocity gradient*, we can express the total mass variation as,

$$\mathrm{d}\dot{m} = \overline{\rho_t J}\mathrm{dV}^0 = \rho_t J \ \mathrm{tr}(\boldsymbol{L}_a)\mathrm{dV}^0 = \mathrm{d}m \ \mathrm{tr}(\boldsymbol{L}_a). \tag{2}$$

In the sequel, the term $\mathrm{tr}\boldsymbol{L}_a$ will be called the *mass production rate* and will be denoted by Γ, i.e.

$$\Gamma = \mathrm{tr}\boldsymbol{L}_a. \tag{3}$$

On the other hand, denoting by $\boldsymbol{v} = \dot{\boldsymbol{x}}$ the velocity vector (i.e. the material derivative of the spatial locations) and by $\nabla_x \cdot$, the divergence operator with respect to the coordinates in the deformed configuration Ω_t, we also have that $\mathrm{d}\dot{m} = (\dot{\rho}_t + \rho_t \nabla_x \cdot \boldsymbol{v})\mathrm{d}m$. By using this identity, the relation $(\dot{\square}) = \frac{\partial \square}{\partial t} + \boldsymbol{v} \cdot \nabla(\square)$, and Eq. (2), we deduce the following equation of mass balance:

$$\frac{\partial \rho_t}{\partial t} + \nabla_x \cdot (\rho_t \boldsymbol{v}) = \rho_t \Gamma.$$

2.2.2 Balance of linear momentum

The total linear momentum $\boldsymbol{p}$ of the solid is defined as,

$$\boldsymbol{p} = \int_{\Omega_t} \rho_t \boldsymbol{v} \ \mathrm{dv} = \int_{\Omega^0} \rho^0 J_a \boldsymbol{v} \ \mathrm{dV}^0.$$

By assuming a field of external body loads per unit of deformed volume $\bar{\boldsymbol{b}}$, the balance of linear momentum reads,

$$\dot{\boldsymbol{p}} = \int_{\Omega_t} \left(\nabla_x \cdot \boldsymbol{\sigma} + \bar{\boldsymbol{b}} \right) \mathrm{dv},$$

where $\boldsymbol{\sigma}$ is the Cauchy stress tensor, and the operator $\nabla_x \cdot$ indicates the divergence with respect to the spatial variables $\boldsymbol{x}$. After introducing the first Piola–Kirchhoff stress tensor $\boldsymbol{P} = J\boldsymbol{F}^{-1}\boldsymbol{\sigma}$, performing the time-derivation of $\boldsymbol{p}$ and resorting to the standard localisation argument (Gonzalez and Stuart 2008), the following balance of linear momentum may be obtained:

$$J_a \rho^0 \left(\dot{\boldsymbol{v}} + \boldsymbol{v}\Gamma \right) = \nabla_0 \cdot \boldsymbol{P} + \bar{\boldsymbol{b}}^0, \tag{4}$$

where the operator $\nabla_0 \cdot$ denotes the divergence with respect to the reference coordinates $\boldsymbol{X}^0$ and $\bar{\boldsymbol{b}}^0 = J\bar{\boldsymbol{b}}$.

2.2.3 Energy balance

Let us define the total internal energy E and the total kinetic energy K of a body as,

$$E := \int_{\Omega_t} \rho_t \phi_t \ \mathrm{dv} = \int_{\Omega^0} \rho^0 \phi^0 \ \mathrm{dV}^0$$

$$K := \int_{\Omega_t} \frac{1}{2} \rho_t \boldsymbol{v} \cdot \boldsymbol{v} \ \mathrm{dv} = \int_{\Omega^0} \frac{1}{2} \rho^0 J_a \boldsymbol{v} \cdot \boldsymbol{v} \ \mathrm{dV}^0,$$

where ϕ_t and $\phi^0 = \phi_t J_a$ are the internal energy per unit of mass in the current and reference configurations, respectively. Variations of ϕ^0 may be due to mechanical (active or passive) or thermal effects. The *balance of thermal and mechanical energy* demands that the time variations of $K + E$ are balanced by thermal fluxes and external loads. In the absence of any external body heating, this becomes

$$\begin{aligned} \dot{E} + \dot{K} &= \int_{\partial\Omega_t} (\bar{\boldsymbol{t}} \cdot \boldsymbol{v} - \boldsymbol{Q} \cdot \boldsymbol{n}) \ \mathrm{da} + \int_{\Omega_t} \bar{\boldsymbol{b}} \cdot \boldsymbol{v} \ \mathrm{dv}, \\ &= \int_{\partial\Omega^0} (\bar{\boldsymbol{t}}^0 \cdot \boldsymbol{v} - \boldsymbol{Q}^0 \cdot \boldsymbol{N}^0) \ \mathrm{dA}^0 + \int_{\Omega^0} \bar{\boldsymbol{b}}^0 \cdot \boldsymbol{v} \ \mathrm{dV}^0, \end{aligned} \tag{5}$$

where $\bar{\boldsymbol{t}}$ and $\boldsymbol{Q}$ are the spatial representations of the external surface loads and thermal fluxes, respectively, and $\bar{\boldsymbol{t}}^0$ and $\boldsymbol{Q}^0$ are their material counterparts. The vectors $\boldsymbol{n}$ and $\boldsymbol{N}^0$ are the outward normals to the body's boundary in the current

and reference configurations. By using the divergence theorem, the boundary condition $\boldsymbol{P}\boldsymbol{N}^0 = \bar{\boldsymbol{t}}^0$ and the localisation argument, Eq. (5) may be expressed as,

$$J_a\rho^0\boldsymbol{v}\cdot\left(\dot{\boldsymbol{v}}+\frac{1}{2}\boldsymbol{v}\Gamma\right)+\rho^0\dot{\phi}^0 = \nabla_0\cdot(\boldsymbol{P}^{\mathrm{T}}\boldsymbol{v})-\nabla_0\cdot\boldsymbol{Q}^0+\bar{\boldsymbol{b}}\cdot\boldsymbol{v}. \tag{6}$$

On the other hand, after pre-multiplying (4) by $\boldsymbol{v}$ and using the relation $\nabla_0\cdot(\boldsymbol{P}^{\mathrm{T}}\boldsymbol{v}) = \boldsymbol{v}\cdot(\nabla_0\cdot\boldsymbol{P})+\nabla_0\boldsymbol{v}:\boldsymbol{P}$ together with the definition $\dot{\boldsymbol{F}} = \nabla_0\boldsymbol{v}$, we can derive the so-called *theorem of kinetic energy* (Maugin and Berezovski 2008):

$$J_a\rho^0\boldsymbol{v}\cdot\dot{\boldsymbol{v}}+J_a\rho^0\boldsymbol{v}\cdot\boldsymbol{v}\Gamma+\boldsymbol{P}:\dot{\boldsymbol{F}} = \nabla_0\cdot(\boldsymbol{P}^{\mathrm{T}}\boldsymbol{v})+\bar{\boldsymbol{b}}\cdot\boldsymbol{v},$$

which subtracted from (6), yields the *First Law of Thermodynamics* (also called theorem of internal energy), which in our case reads,

$$\rho^0\dot{\phi}^0 = \frac{1}{2}J_a\rho^0\boldsymbol{v}\cdot\boldsymbol{v}\Gamma+\boldsymbol{P}:\dot{\boldsymbol{F}}-\nabla_0\cdot\boldsymbol{Q}^0. \tag{7}$$

2.3 Thermodynamics

The motivation of this section is the construction of proper constitutive laws for the elastic and active parts of the deformation, which are thermodynamically consistent. We first present some general well-known facts that we particularise to our needs in the model.

2.3.1 Reduced dissipation inequality

The balance of entropy for the open system balances the entropy density rate per unit of reference volume $\dot{S}$, minus an extra entropy source $\bar{S}$ (which accounts for the contribution of the mass transferred to the system, see for instance Kuhl and Steinmann (2003), Himpel et al. (2005), with an external contribution h_{ext}, plus a internal contribution $h_{int}\geq 0$, that is,

$$\dot{S}-\bar{S} = h_{ext}+h_{int}.$$

From the non-negativity of h_{int} and the expression of the external contribution as $h_{ext} = \nabla_0\cdot(\frac{-\boldsymbol{Q}^0}{\Theta})$, with $\Theta>0$ the absolute temperature, the *Second Law of thermodynamics* follows as (Gonzalez and Stuart 2008; Holzapfel 2000; Maugin and Berezovski 2008),

$$\dot{S}+\nabla_0\cdot\left(\frac{\boldsymbol{Q}^0}{\Theta}\right)-\bar{S}\geq 0. \tag{8}$$

Inserting Eq. (7) into (8) yields the following alternative expression of the second law:

$$\Theta\dot{S}+J_a\rho^0\frac{1}{2}\boldsymbol{v}\cdot\boldsymbol{v}\Gamma+\boldsymbol{P}:\dot{\boldsymbol{F}}-\rho^0\dot{\phi}^0 -\frac{\boldsymbol{Q}^0}{\Theta}\cdot\nabla_0\Theta-\Theta\bar{S}\geq 0. \tag{9}$$

Relations (7) and (9) may be rewritten by using the Helmholtz free energy function per unit of mass ψ^0, such that $\rho^0\psi^0(\boldsymbol{F},\Theta) = \rho^0\phi^0(\boldsymbol{F},S)-S\Theta$, which is the Legendre transformation of $\phi^0(\boldsymbol{F},S)$ with respect to S, with $\Theta = \frac{\partial\rho^0\psi^0(\boldsymbol{F},S)}{\partial S}$. In this way, we may write inequality (9) in the following convenient form:

$$\boldsymbol{P}:\dot{\boldsymbol{F}}+J_a\rho^0\frac{1}{2}\boldsymbol{v}\cdot\boldsymbol{v}\Gamma-\rho^0\dot{\psi}^0 -\frac{\boldsymbol{Q}^0}{\Theta}\cdot\nabla_0\Theta-\dot{\Theta}S-\Theta\bar{S}\geq 0. \tag{10}$$

Since no temperature variations have been reported in the morphogenesis processes studied here, which occur at relatively slow speed, we will neglect in the remainder of the paper thermal and inertial effects, that is, we assume $\Theta\approx constant$, $\boldsymbol{Q}^0\approx\boldsymbol{0}$ and $\rho^0\boldsymbol{v}\approx 0$, and therefore we will use a quasi-static approximation of the process. With these hypotheses, Eq. (10) turns into the so-called *reduced dissipation inequality*,

$$\mathcal{D} := \boldsymbol{P}:\dot{\boldsymbol{F}}-\rho^0\dot{\psi}^0-\Theta\bar{S}\geq 0, \tag{11}$$

where $\mathcal{D}$ is the dissipated energy. Equation (11) furnishes the necessary conditions that any constitutive law relating all admissible values of $\dot{\boldsymbol{F}}$ and $\boldsymbol{P}$ should satisfy.

2.3.2 Introducing active deformations

In the subsequent derivations, we will assume that configuration Ω^0 is stress-free and that the free energy function per unit of *intermediate* volume $\psi = J_a^{-1}\psi^0$ is a function of the passive deformations gradient $\boldsymbol{F}_e$. For completeness, we will also assume that ψ depends as well on the active deformations $\boldsymbol{F}_a$, i.e. $\psi = \psi(\boldsymbol{F}_a,\boldsymbol{F}_e)$. The latter assumption gives rise to an active stress tensor given by $\boldsymbol{S}_a = \frac{\partial\psi}{\partial\boldsymbol{F}_a}$, and therefore yields a configuration Ω that might not be stress-free.

Although the explicit form of $\psi(\boldsymbol{F}_a,\boldsymbol{F}_e)$ is at this point left undetermined, it is interesting, among the several possible choices, to split it in two terms, which additively superimpose to form $\psi(\boldsymbol{F}_a,\boldsymbol{F}_e) = \psi_e(\boldsymbol{F}_e)+\psi_a(\boldsymbol{F}_a)$. In this case, ψ_e accounts for the elastic energy stored in the solid, whereas ψ_a represents the energy stored in the chemical bonds of the structural elements of the cell, and thus its variation is associated to changes in $\boldsymbol{F}_a$. Similar decompositions may be found in Garikipati et al. (2006), where the active (remodelling) deformations are due to a particular dependence of ψ on the fibre reorientation. A discussion on the interpretation of the active deformations in the case of structural elements of the cell is given in Sect. 3.

It is convenient to recast the reduced dissipation inequality in (11) by rewriting it as a function of the free energy per unit of mass in the intermediate configuration $\psi(\boldsymbol{F}_a,\boldsymbol{F}_e) =$

$J_a^{-1}\psi^0(\boldsymbol{F}_a, \boldsymbol{F}_e)$ as follows:

$$\boldsymbol{P} : \dot{\boldsymbol{F}} - \rho^0 (J_a \psi)^{\cdot} - \Theta \bar{S} \geq 0. \tag{12}$$

By recalling that $\rho = \rho^0 =$ constant when passing from Ω^0 to Ω and by resorting to the relations $\dot{J}_a = J_a \boldsymbol{F}_a^{-\mathrm{T}} : \dot{\boldsymbol{F}}_a$ and $\dot{\boldsymbol{F}}_e = \dot{\boldsymbol{F}}\boldsymbol{F}_a^{-1} - \boldsymbol{F}_e \dot{\boldsymbol{F}}_a \boldsymbol{F}_a^{-1}$, it follows that $(J_a\psi)^{\cdot}$ in (12) is given by:

$$\begin{aligned}(J_a\psi)^{\cdot} &= J_a \frac{\partial \psi}{\partial \boldsymbol{F}_a} : \dot{\boldsymbol{F}}_a + J_a \frac{\partial \psi}{\partial \boldsymbol{F}_e} : \dot{\boldsymbol{F}}_e + J_a \psi \boldsymbol{F}_a^{-T} : \dot{\boldsymbol{F}}_a \\ &= J_a \left(\psi \boldsymbol{I} + \frac{\partial \psi}{\partial \boldsymbol{F}_a} \boldsymbol{F}_a^{\mathrm{T}} - \boldsymbol{F}_e^{\mathrm{T}} \frac{\partial \psi}{\partial \boldsymbol{F}_e} \right) : \boldsymbol{L}_a \\ &\quad + J_a \frac{\partial \psi}{\partial \boldsymbol{F}_e} : \dot{\boldsymbol{F}} \boldsymbol{F}_a^{-1}. \end{aligned} \tag{13}$$

By inserting this relation into Eq. (12) and using the fact that the inequality must be satisfied for all admissible deformations $\boldsymbol{F}_a$ and $\boldsymbol{F}$, it follows that the stress tensor $\boldsymbol{P}$ is given by,

$$\boldsymbol{P} = \rho^0 J_a \frac{\partial \psi}{\partial \boldsymbol{F}_e} \boldsymbol{F}_a^{-\mathrm{T}} = J_a \boldsymbol{P}_e \boldsymbol{F}_a^{-\mathrm{T}}, \tag{14}$$

where the stress $\boldsymbol{P}_e = \rho^0 \frac{\partial \psi}{\partial \boldsymbol{F}_e}$ is the push-forward of the first Piola–Kirchhoff stress tensor $\boldsymbol{P}$. From the identity (14) and the expression in (13), the reduced dissipation inequality in (12) furnishes the following relationship:

$$\begin{aligned}\mathcal{D} = J_a \boldsymbol{F}_e^{\mathrm{T}} \boldsymbol{P}_e : \boldsymbol{L}_a - J_a \rho^0 \left(\psi \boldsymbol{I} + \frac{\partial \psi}{\partial \boldsymbol{F}_a} \boldsymbol{F}_a^{\mathrm{T}} \right) : \boldsymbol{L}_a \\ - \Theta \bar{S} \geq 0. \end{aligned} \tag{15}$$

We note that the tensor $\boldsymbol{F}_e^{\mathrm{T}} \boldsymbol{P}_e$ is referred to in the literature as the Mandel stress tensor (Epstein and Maugin 2000; Himpel et al. 2005; Holzapfel 2000; Steinmann 2002).

2.4 Equilibrium equations

Three approaches may be pursued when deriving the equilibrium equations in the presence of active elongation: (i) Noether's theorem, (ii) the Virtual Power Principle (VPP), or (iii) the minimisation of an energy functional (variational method). Methods (i) and (ii) are omitted here, but the reader may find the necessary steps in Kienzler and Herrmann (2000) and DiCarlo and Quiligotti (2002), Ambrosi and Guana (2007)), respectively. Method (ii) is convenient when, due to the incompatibility of the intermediate configuration Ω, the map $\boldsymbol{X}(\boldsymbol{X}^0, t) : \Omega^0 \to \Omega$ is not compatible, not even piecewise, and therefore $\boldsymbol{u}_a = \boldsymbol{X} - \boldsymbol{X}^0$ and $\boldsymbol{u}_e = \boldsymbol{x} - \boldsymbol{X}$ are not defined. In this case, method (iii) may not be applicable, and the tensor $\boldsymbol{F}_a$ and the deformation gradient $\boldsymbol{F} = \frac{\partial \boldsymbol{u}}{\partial \boldsymbol{X}^0}$ are taken as the primary kinematic variables. If we assume $\boldsymbol{u}_a$ and $\boldsymbol{u}_e$ are defined, method (iii) consists on interpreting the tensors $\boldsymbol{F}_a$ and $\boldsymbol{F}_e$ as displacement gradients, respectively, given by $\boldsymbol{F}_a = \frac{\partial \boldsymbol{u}_a}{\partial \boldsymbol{X}^0}$ and $\boldsymbol{F}_e = \frac{\partial \boldsymbol{u}_e}{\partial \boldsymbol{X}}$. In this case, we can write the free energy function as $\psi(\boldsymbol{u}_a, \boldsymbol{u}_e)$ and find the equilibrium process as the minimisation of a functional. The choice of method (iii) is motivated by the fact that the subsequent equations are applied to unidimensional elements (bars) in Sect. 3, where it is reasonable to assume that the displacement fields $\boldsymbol{u}_a$ and $\boldsymbol{u}_e$ exist, at least piecewise.

We neglect any body loads $\bar{\boldsymbol{b}}$ but consider an external force $\bar{\boldsymbol{t}}$ on the boundary $\partial\Omega_t$. Using a free energy density function per unit of intermediate mass $\psi(\boldsymbol{u}_a, \boldsymbol{u}_e)$ and noting $\rho = \rho^0$ in Ω, the spatial equilibrium equations are obtained by minimising the following energy functional with respect to the active and elastic displacements $\boldsymbol{u}_a$ and $\boldsymbol{u}_e$:

$$\Pi(\boldsymbol{u}_a, \boldsymbol{u}_e) = \int_{\Omega} \rho^0 \psi(\boldsymbol{u}_a, \boldsymbol{u}_e) \, \mathrm{dV} - \int_{\partial\Omega_t} \bar{\boldsymbol{t}} \cdot \boldsymbol{u} \, \mathrm{da}, \tag{16}$$

or equivalently, solving the following variational equation:

$$\delta\Pi = \frac{d}{d\epsilon} \Pi(\boldsymbol{u}_a + \epsilon \delta\boldsymbol{u}_a, \boldsymbol{u}_e + \epsilon \delta\boldsymbol{u}_e)\Big|_{\epsilon=0} = 0. \tag{17}$$

Note that the functional does not depend on the time derivatives of $\boldsymbol{u}_a$ or $\boldsymbol{u}_e$, and we are therefore neglecting any inertial terms.

A general expression for $\delta\Pi$ may be obtained by resorting to the minimisation of the total virtual work in a manner similar to the time differentiation performed on ψ in Sect. 2.3. By doing so, the following equation is obtained:

$$\begin{aligned}\delta\Pi = \int_{\Omega} \rho^0 \left(\frac{\partial \psi}{\partial \boldsymbol{F}_a} : \delta\boldsymbol{F}_a + \frac{\partial \psi}{\partial \boldsymbol{F}_e} : \delta\boldsymbol{F}_e + \psi \boldsymbol{F}_a^{-T} : \delta\boldsymbol{F}_a \right) \mathrm{dV} \\ - \int_{\partial\Omega_t} \bar{\boldsymbol{t}} \cdot \delta\boldsymbol{u} \, \mathrm{da} = 0, \quad \forall \delta\boldsymbol{u}_a, \delta\boldsymbol{u}_e. \end{aligned} \tag{18}$$

In view of the following relations:

$$\begin{aligned}\delta(\boldsymbol{F}_e) &= (\delta\boldsymbol{F})\boldsymbol{F}_a^{-1} - \boldsymbol{F}_e(\delta\boldsymbol{F}_a)\boldsymbol{F}_a^{-1}, \\ (\delta\boldsymbol{F})\boldsymbol{F}_a^{-1} &= \frac{\partial \delta\boldsymbol{u}}{\partial \boldsymbol{X}^0} \frac{\partial \boldsymbol{X}^0}{\partial \boldsymbol{X}} = \frac{\partial \delta\boldsymbol{u}}{\partial \boldsymbol{X}}, \\ (\delta\boldsymbol{F}_a)\boldsymbol{F}_a^{-1} &= \frac{\partial \delta\boldsymbol{u}_a}{\partial \boldsymbol{X}^0} \frac{\partial \boldsymbol{X}^0}{\partial \boldsymbol{X}} = \frac{\partial \delta\boldsymbol{u}_a}{\partial \boldsymbol{X}}, \end{aligned}$$

the first integral in (18) can be rewritten in terms of the virtual displacements $\delta\boldsymbol{u}$ and $\delta\boldsymbol{u}_a$ as,

$$\begin{aligned}\delta\Pi = \int_{\Omega} \rho^0 \left(\frac{\partial \psi}{\partial \boldsymbol{F}_a} \boldsymbol{F}_a^{\mathrm{T}} - \boldsymbol{F}_e^{\mathrm{T}} \frac{\partial \psi}{\partial \boldsymbol{F}_e} + \psi \boldsymbol{I} \right) : \frac{\partial \delta\boldsymbol{u}_a}{\partial \boldsymbol{X}} \, \mathrm{dV} \\ + \int_{\Omega} \frac{\partial \psi}{\partial \boldsymbol{F}_e} : \frac{\partial \delta\boldsymbol{u}}{\partial \boldsymbol{X}} \, \mathrm{dV} - \int_{\partial\Omega_t} \bar{\boldsymbol{t}} \cdot \delta\boldsymbol{u} \, \mathrm{da}. \end{aligned} \tag{19}$$

With the aim of considering a coupling between the active and passive deformations, we will next deduce from this expression the equilibrium equations in the following three situations:

(a) *Unconstrained deformation*: The active and passive displacements, $\boldsymbol{u}_a$ and $\boldsymbol{u}_a$, are independent. In consequence, the corresponding virtual displacements $\delta\boldsymbol{u}_a$ and $\delta\boldsymbol{u}_a$ are also independent.
(b) *Fixed deformed configuration*: The passive and active displacements are free to vary, but the final configuration Ω_t is fixed, i.e. $\delta\boldsymbol{u} = \boldsymbol{0}$.
(c) *Coupled deformation*: A relation exists between the passive and active displacements, that is, we consider two dependent fields of virtual displacements $\delta\boldsymbol{u}_a$ and $\delta\boldsymbol{u}_e$.

2.4.1 Unconstrained deformation

From the arbitrariness of the virtual displacements $\delta\boldsymbol{u}$ and $\delta\boldsymbol{u}_a$ in (19), we obtain, after integrating by parts and using the definition $\boldsymbol{P}_e = \rho^0 \frac{\partial \psi}{\partial \boldsymbol{F}_e}$, the following set of differential equations:

$$\nabla_X \cdot \left(\rho^0 \frac{\partial \psi}{\partial \boldsymbol{F}_a} \boldsymbol{F}_a^{\mathrm{T}} - \boldsymbol{F}_e^{\mathrm{T}} \boldsymbol{P}_e + \rho^0 \psi \boldsymbol{I} \right) = \boldsymbol{0}, \quad \forall \boldsymbol{X} \in \Omega \tag{20a}$$

$$\nabla_X \cdot \boldsymbol{P}_e = \boldsymbol{0}, \quad \forall \boldsymbol{X} \in \Omega \tag{20b}$$

$$\rho^0 \left(\frac{\partial \psi}{\partial \boldsymbol{F}_a} \boldsymbol{F}_a^{\mathrm{T}} \boldsymbol{N} + \psi \boldsymbol{N} \right) = \boldsymbol{F}_e^{\mathrm{T}} \boldsymbol{P}_e \boldsymbol{N}, \quad \forall \boldsymbol{X} \in \partial\Omega \tag{20c}$$

$$\boldsymbol{P}_e \boldsymbol{F}_e^{\mathrm{T}} \boldsymbol{n} = J_e \bar{\boldsymbol{t}}, \quad \forall \boldsymbol{x} \in \partial\Omega_t, \tag{20d}$$

where in the last equation, we have used Nanson's formula: $\boldsymbol{N}\mathrm{dA} = J_e^{-1} \boldsymbol{F}_e^{\mathrm{T}} \boldsymbol{n}\,\mathrm{da}$, with $\boldsymbol{N}$ and $\boldsymbol{n}$ the normal vectors in the intermediate and deformed configurations, respectively. The operator $\nabla_X \cdot$ denotes the divergence with respect to the coordinates in the intermediate configuration.

We remark that Eqs. (20b) and (20d) are the standard balance of linear momentum (in the material setting), whereas (20a) and (20c) are the equilibrium equations due to configurational changes. The latter were originally introduced by Eshelby 1951 and are coined in the literature as configurational balance equations (Gurtin 2000) or balance of pseudo-momentum (Maugin 1995). In our notation, Eq. (20a) must be satisfied for all changes of the intermediate configuration. Therefore, and in view of Eq. (19), when Ω is fixed (i.e. $\delta\boldsymbol{u}_a = \boldsymbol{0}$), no such equations are obtained.

2.4.2 Fixed deformed configuration

We here derive the resulting equations for a body whose whole deformation is fixed, i.e. $\delta\boldsymbol{u} = \boldsymbol{0}$, but with variable active and elastic displacements.

After using the condition $\delta\boldsymbol{u} = \boldsymbol{0}$, the second row of Eq. (19) vanishes, and therefore the expression of $\delta\Pi$ reads:

$$\delta\Pi = \int_{\Omega} \rho^0 \left(\frac{\partial \psi}{\partial \boldsymbol{F}_a} \boldsymbol{F}_a^{\mathrm{T}} - \boldsymbol{F}_e^{\mathrm{T}} \frac{\partial \psi}{\partial \boldsymbol{F}_e} + \psi \boldsymbol{I} \right) : \frac{\partial \delta \boldsymbol{u}_a}{\partial \boldsymbol{X}}\,\mathrm{dV}.$$

Resorting to the divergence theorem and recalling that $\boldsymbol{P}_e = \rho^0 \frac{\partial \psi}{\partial \boldsymbol{F}_e}$, the expression above yields the equilibrium equations in (20a) and (20c). Therefore, as a result, it turns out that the latter are the balance conditions that any motion must satisfy when the deformed configuration is fully constrained ($\delta\boldsymbol{u} = \boldsymbol{0}$), but with a changing intermediate configuration, or equivalently, with a change in the internal structure. It is thus reasonable that the Eshelby tensor $\psi \boldsymbol{I} - \boldsymbol{F}_e^{\mathrm{T}} \frac{\partial \psi}{\partial \boldsymbol{F}_e}$ makes it appearance in the equilibrium equations.

We note that the same result would be obtained if we inserted into Eq. (18) the relation,

$$\delta \boldsymbol{F}_e = -\boldsymbol{F}_e \delta \boldsymbol{F}_a \boldsymbol{F}_a^{-1} = -\boldsymbol{F}_e \frac{\partial \delta \boldsymbol{u}_a}{\partial \boldsymbol{X}}, \tag{21}$$

which follows from the condition $\delta\boldsymbol{F} = \boldsymbol{0}$.

2.4.3 Coupled deformation

Motivated by experimental observations, we here postulate that the active displacements $\boldsymbol{u}_a$ depend on the elastic displacements $\boldsymbol{u}_e$ via the corresponding deformation gradients, $\boldsymbol{F}_a$ and $\boldsymbol{F}_e$. We write this dependence by introducing a *control function* that relates the active and elastic deformations as follows:

$$\dot{\boldsymbol{F}}_a = \boldsymbol{C}(\boldsymbol{F}_e). \tag{22}$$

We henceforth remove for clarity the dependence of the tensorial function $\boldsymbol{C}$ on $\boldsymbol{F}_e$, and an explicit expression is given for $\boldsymbol{C}$ in Sect. 3. This equation couples both components of the decomposition of the deformation gradient, which has the following two main implications:

1. The evolution law for $\boldsymbol{F}_a$ in (22) induces an expression of the gradient of the active velocity $\boldsymbol{L}_a$, which inserted into condition (15), determines the amount of dissipated energy $\mathcal{D}$.
2. The spatial and material equilibrium equations are now coupled due to the coupling introduced in (22) and yield a single equilibrium equation. This dependence is treated in a similar manner as the constraint $\delta\boldsymbol{u} = \boldsymbol{0}$ introduced in Sect. 2.4.

Regarding point 1 above, we note that due to Eq. (22), the velocity gradient is now given by $\boldsymbol{L}_a = \dot{\boldsymbol{F}}_a \boldsymbol{F}_a^{-1} = \boldsymbol{C}\boldsymbol{F}_a^{-1}$. By inserting this expression into the mass production rate in (3) and the dissipation energy in (15), we may write these equations as,

$$\begin{aligned} &\Gamma = \mathrm{tr}(\boldsymbol{C}\boldsymbol{F}_a^{-1}), \\ &J_a \left(\boldsymbol{F}_e^{\mathrm{T}} \boldsymbol{P}_e - \rho^0 \left(\psi \boldsymbol{I} + \frac{\partial \psi}{\partial \boldsymbol{F}_a} \boldsymbol{F}_a^{\mathrm{T}} \right) \right) : \boldsymbol{C}\boldsymbol{F}_a^{-1} - \Theta \bar{S} \geq 0. \end{aligned} \tag{23}$$

As a consequence, the condition $\mathcal{D} \geq 0$ imposes some restrictions on the plausible expressions of $\boldsymbol{C}$, which will be analysed in the next sections.

With regard to point 2 stated above, it is convenient to discretise in time Eq. (22). We perform this task by introducing the following time-stepping,

$$\boldsymbol{F}_{a,n+1} = \boldsymbol{F}_{a,n} + \Delta t \boldsymbol{C}_{n+\theta}, \tag{24}$$

where $\boldsymbol{C}_{n+\theta} = \boldsymbol{C}(\boldsymbol{F}_{e,n+\theta}), 0 \geq \theta \geq 1, (\square)_{n+\theta} = (1-\theta)(\square)_n + \theta(\square)_{n+1}$ and $\Delta t = t_{n+1} - t_n$. The values $\theta = 0, 1/2, 1$ correspond to the standard forward Euler, mid-point rule or backward Euler, respectively. It is shown in Appendix A that in all these cases, the relation in (24) allows us to write the following relation between the virtual deformation gradients:

$$\delta \boldsymbol{F}_a = \boldsymbol{\mathcal{L}} : \delta \boldsymbol{F}, \tag{25}$$

This relationship may be interpreted as a constriction on the motion, in a similar manner to Eq. (21) in the case with a fixed deformation. Inserting relation (25) into Eq. (19), the following equilibrium equation can be derived,

$$\nabla_X \cdot \left(\boldsymbol{P}_e + \left(\rho^0 \frac{\partial \psi}{\partial \boldsymbol{F}_a} \boldsymbol{F}_a^{\mathrm{T}} + \rho^0 \psi \boldsymbol{I} - \boldsymbol{F}_e^{\mathrm{T}} \boldsymbol{P}_e \right) \boldsymbol{F}_a^{-\mathrm{T}} : \boldsymbol{\mathcal{L}} \boldsymbol{F}_a^{\mathrm{T}} \right) = \boldsymbol{0}, \quad \forall \boldsymbol{X} \in \Omega, \tag{26}$$

which should be complemented with the corresponding boundary conditions. Clearly, this equation differs from the standard elastic equilibrium in (20b). While other references such as Rodriguez et al. (1994), Taber (2008), Ramasubramanian and Taber (2008) model growth by solving Eq. (20b) in parallel with an evolution law for $\boldsymbol{F}_a$, we also apply this evolution law but in conjunction with Eq. (26), which fully couples the elastic equilibrium in (20b) and the configurational balance equations (20a).

In the next Section, we apply these ideas to a system of unidimensional bars in order to model stress-controlled morphogenesis. We show that some of the terms in (26) simplify substantially.

3 Mechanics of trusses

We here particularise the decomposition and equilibrium equations described in the previous sections to a system of trusses, composed by bars connected at their ends. We also decompose the motion of each bar element into an active elongation and an elastic deformation. In the context of cellular deformations, the active elongation may be seen as the inclusion of new parts of the actin helix onto which the myosin head is sliding. The elastic deformation is instead the result of applying some external forces $\bar{\boldsymbol{q}}$ or the compatibility of the joints with other bars connected at its ends (see Fig. 2). The growth process and the elastic deformation will eventually cause the whole bar to reorient, and therefore produce a remodelling of the cell, and as a by-product, change the global shape of the cell and the epithelium. The examples analysed in Sect. 4 will illustrate this sequence of events.

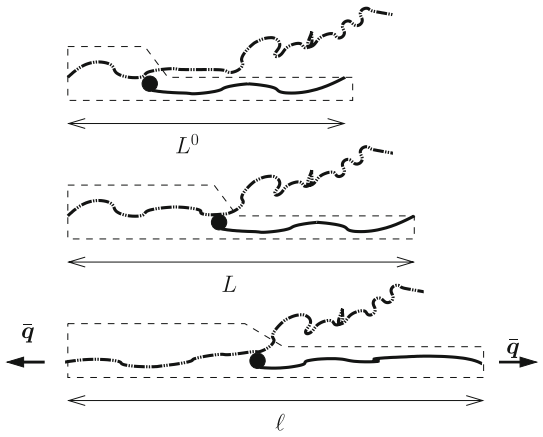

Fig. 2 Representation of the three configurations for an actin–myosin complex. The biological system modelled through a single bar is represented by the actin–myosin chain portion outlined by the *dashed line*. The reference, intermediate and deformed lengths of the system, respectively, denoted by L^0, L and ℓ are also indicated in the *Figure*. Due to the movement of the myosin head along the actin helix, new mass enters the system at constant density as the chain length changes from L^0 to L and the system moves from the initial configuration Ω^0 to the intermediate Ω (see Sect. 2.2)

3.1 Bar kinematics

The bar elements employed in our model are defined by the following kinematic assumptions:

- Each bar is a body much longer in one direction that in the other 2 perpendicular directions.
- The bar remains as a straight body in all the configurations, with a constant area.
- The cross-section of the bar remains perpendicular to the centroid axis and has a constant area.
- The bar in the reference configuration is oriented in such a way that its long axis is parallel to the vector $\boldsymbol{E}_1$ of a reference triad (see Fig. 3).
- The active deformations deform the bar only in the longitudinal direction, that is in the direction of $\boldsymbol{E}_1$. Also, and in agreement with our hypothesis in the three-dimensional case, no density changes occur during this active deformation.
- The elastic deformations correspond to a change in the longitudinal along $\boldsymbol{E}_1$ axis plus a rotation $\boldsymbol{R}$, constant for each bar.

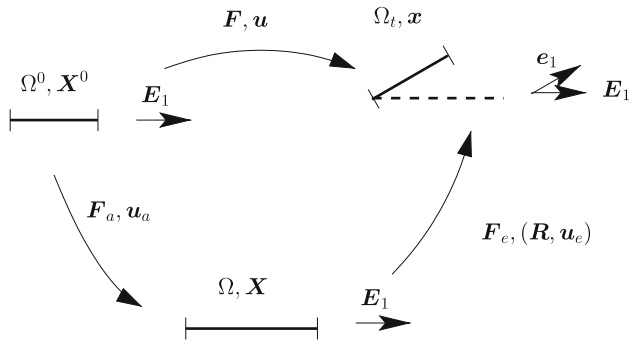

Fig. 3 Maps between the reference, intermediate and deformed configurations for each *bar* element

Such a motion of the bar is visualised with the maps indicated in Fig. 3. The positions of the material point in each configuration are accordingly given by,

$$\boldsymbol{X}^0 = X_i^0 \boldsymbol{E}_i$$
$$\boldsymbol{X} = X_i \boldsymbol{E}_i$$
$$\boldsymbol{x} = x_i \boldsymbol{e}_i = x_i \boldsymbol{R} \boldsymbol{E}_i$$

where $\boldsymbol{R}$ is a rotation matrix that transforms the vector $\boldsymbol{E}_i$ into $\boldsymbol{e}_i$, i.e. $\boldsymbol{R} = \boldsymbol{e}_i \otimes \boldsymbol{E}_i$ and $\boldsymbol{e}_i = \boldsymbol{R}\boldsymbol{E}_i$. We remark that in the previous equations we do not constrain the material points to be only along the axis $\boldsymbol{E}_1$ (the bar is assumed slender, but the area of the cross-section is not zero). From the kinematic assumptions, the three configurations are related through the following relations:

$$\begin{aligned} \boldsymbol{X} &= \boldsymbol{X}^0 + u_a(X_1^0)\boldsymbol{E}_1 = u_a(X_1^0)\boldsymbol{E}_1 + X_i^0 \boldsymbol{E}_i \\ \boldsymbol{x} &= \boldsymbol{R}(\boldsymbol{X} + u_e(X_1)\boldsymbol{E}_1) = u_e(X_1)\boldsymbol{e}_1 + X_i \boldsymbol{e}_i \\ &= (u_a(X_1^0) + u_e(X_1))\boldsymbol{e}_1 + X_i^0 \boldsymbol{e}_i, \end{aligned} \tag{27}$$

where summation on the repeated subscript $i = 1, 2, 3$ must be understood. The scalar functions $u_a(X_1^0)$ and $u_e(X_1)$ are the active and passive displacements, respectively, which determine the corresponding deformations in the intermediate and deformed configurations.

We denote by $[0, L^0]$, $[0, L]$ and $[0, \ell]$ the domains of X_1^0, X_1 and x_1, respectively. The values L^0, L and ℓ correspond to the lengths of the bars in the reference, intermediate and deformed configurations, respectively. The expressions of the deformation gradients may be then written as,

$$\begin{aligned} \boldsymbol{F}_a &= \frac{\partial \boldsymbol{X}}{\partial \boldsymbol{X}^0} = u_a' \boldsymbol{E}_1 \otimes \boldsymbol{E}_1 + \boldsymbol{E}_i \otimes \boldsymbol{E}_i \\ \boldsymbol{F}_e &= \frac{\partial \boldsymbol{x}}{\partial \boldsymbol{X}} = u_e' \boldsymbol{e}_1 \otimes \boldsymbol{E}_1 + \boldsymbol{e}_i \otimes \boldsymbol{E}_i \\ \boldsymbol{F} &= \frac{\partial \boldsymbol{x}}{\partial \boldsymbol{X}^0} = u' \boldsymbol{e}_1 \otimes \boldsymbol{E}_1 + \boldsymbol{e}_i \otimes \boldsymbol{E}_i. \end{aligned} \tag{28}$$

In the last equation, we have introduced a scalar function $u(X_1^0)$ that, after comparing the last equations in (27) and (28), is defined by the following equality:

$$\begin{aligned} 1 + u' &= 1 + u_a' + u_e' \frac{\partial X_1}{\partial X_1^0} = 1 + u_a' + u_e' + u_e' u_a' \\ &= (1 + u_a')(1 + u_e'). \end{aligned} \tag{29}$$

In view of this result and the expression in (28), it is easy to verify that the multiplicative decomposition $\boldsymbol{F} = \boldsymbol{F}_e \boldsymbol{F}_a$ holds. Note that $u_a' = \frac{\partial u_a}{\partial X_1^0}$ and $u' = \frac{\partial u}{\partial X_1^0}$, but $u_e' = \frac{\partial u_e}{\partial X_1}$.

The associated strain and stress measures of the bars are obtained by particularising the expression of the elastic power $\dot{W} = \int_{L^0} \boldsymbol{P} : \dot{\boldsymbol{F}} \, \mathrm{d}X_1^0$, to the kinematic assumptions mentioned earlier. It is demonstrated in Appendix B that using the kinematic assumptions of the bar, $\dot{W}$ may be expressed as,

$$\dot{W} = \int_{L^0} \boldsymbol{q} \cdot \dot{\boldsymbol{\varepsilon}} \, \mathrm{d}X_1^0 = \int_L (1 + u_a')^{-1} \boldsymbol{q} \cdot \dot{\boldsymbol{\varepsilon}} \, \mathrm{d}X_1 \tag{30}$$

where $\boldsymbol{\varepsilon} = (1 + u')\boldsymbol{E}_1$ and $\boldsymbol{q} = \boldsymbol{R}^{\mathrm{T}} \int_{A^0} \boldsymbol{P}_1 dA^0$. Here, the vector $\boldsymbol{P}_1$ is the tension in the deformed configuration per unit of area A^0 perpendicular to vector $\boldsymbol{E}_1$ of the reference configuration. Consequently, $\boldsymbol{q}$ corresponds to the axial force in the deformed bar, but rotated back in the direction $\boldsymbol{E}_1$. We note that the stress and strain measures obtained for the bars are those of the geometrically exact beam theory (Simo 1985), but with no bending stiffness. We also remark that the obtained strain measure $\dot{\boldsymbol{\varepsilon}}(1 + u_a')^{-1}$ mimics the tensor product $\dot{\boldsymbol{F}}\boldsymbol{F}_a^{-1}$ in the three-dimensional case.

In general, we assume that the free energy of the bar ψ depends on the elastic strain measure $\gamma_e = 1 + u_e'$ and an active deformation $\gamma_a = 1 + u_a'$. The relation between those measures and the deformation $\gamma = \boldsymbol{\varepsilon} \cdot \boldsymbol{E}_1 = 1 + u'$ in (30) is obtained from the relations of the displacement derivatives in (29), i.e.

$$\gamma = \gamma_a \gamma_e, \tag{31}$$

which is a scalar version of the deformation gradient decomposition $\boldsymbol{F} = \boldsymbol{F}_e \boldsymbol{F}_a$.

3.2 Constitutive law

Proceeding like in the three-dimensional case, the reduced dissipation inequality in (15) yields, after recalling that $\boldsymbol{P} : \dot{\boldsymbol{F}}$ is equivalent to the product $\boldsymbol{q} \cdot \dot{\boldsymbol{\varepsilon}}$, the following expression:

$$\mathcal{D} = \left(\gamma_e q_e - \rho^0 \left(\psi + \frac{\partial \psi}{\partial \gamma_a} \gamma_a \right) \right) \dot{\gamma}_a - \Theta \bar{S} \geq 0, \tag{32}$$

where we have introduced the stress scalar $q_e = \rho^0 \frac{\partial \psi}{\partial \gamma_e} = \gamma_a \boldsymbol{q} \cdot \boldsymbol{E}_1$, with $\boldsymbol{q} = \rho^0 \frac{\partial \psi}{\partial \gamma} \boldsymbol{E}_1$.

3.3 Equilibrium equations

3.3.1 Unconstrained deformations

It has been shown in Sect. 2.4 that when allowing independent virtual displacements $\delta \boldsymbol{u}_a$ and $\delta \boldsymbol{u}_e$, the equilibrium equations in (20) are obtained. We here use the same methodology assuming an external point load $\bar{\boldsymbol{q}}$ at the bar ends, and the following energy functional, equivalent to the one in (16):

$$\Pi = \int_L \rho^0 \psi \, \mathrm{d}X_1 - \bar{\boldsymbol{q}} \cdot \boldsymbol{u} \Big|_{x_1=0}^{x_1=\ell},$$

where $\boldsymbol{u} = u\boldsymbol{e}_1$. The minimisation of Π above, noting that $\delta \boldsymbol{e}_1 = (u\widehat{\delta \boldsymbol{w}} + \delta u \boldsymbol{I})\boldsymbol{e}_1$, with $\widehat{\delta \boldsymbol{w}}$ a skew-symmetric matrix (see Appendix B), yields the following equilibrium equations:

$$\frac{\partial}{\partial X_1}\left(\rho^0 \frac{\partial \psi}{\partial \gamma_a}(1+u_a') + \rho^0 \psi - \gamma_e q_e\right) = 0, \quad \forall X_1 \in [0, L] \tag{33a}$$

$$\frac{\partial}{\partial X_1} q_e = 0, \quad \forall X_1 \in [0, L] \tag{33b}$$

$$\rho^0 \frac{\partial \psi}{\partial \gamma_a}\gamma_a + \rho^0 \psi - \gamma_e q_e = 0, \quad \text{at} \quad X_1 = \{0, L\} \tag{33c}$$

$$q_e = \bar{\boldsymbol{q}} \cdot \boldsymbol{n}, \quad \text{at} \quad x_1 = \{0, \ell\} \tag{33d}$$

$$\bar{\boldsymbol{q}} = (\bar{\boldsymbol{q}} \cdot \boldsymbol{e}_1)\boldsymbol{e}_1 \tag{33e}$$

where now $\boldsymbol{n}\big|_{X_1=L} = \boldsymbol{e}_1 = -\boldsymbol{n}\big|_{X_1=0}$. Equations (33b) and (33d) are the standard spatial equations due to the variations $\delta \boldsymbol{u}$, which state that the axial load q_e is constant along the bar and equal to the values of the external load applied at the bar ends. Equation (33e) imposes the condition that the external load must be aligned to vector $\boldsymbol{e}_1$.

When dealing with a truss system of I bars and J joints, the local equilibrium Eqs. (33a) and (33b) are applied to each bar $i = 1, \ldots, I$, whereas the boundary conditions (33d–33e) must be replaced by the static equilibrium at each joint $j = 1, \ldots, J$, that is

$$\sum_{i \in j} q_e^{ij} \boldsymbol{R}^i \boldsymbol{E}_1 = \bar{\boldsymbol{q}}^j, \quad j = 1, \ldots, J \tag{33f}$$

where the sum is performed over all the elements i connected to joint j, q_e^{ij} is the elastic stress of each bar i connected to joint j, $\bar{\boldsymbol{q}}^j$ is the external load at joint j and $\boldsymbol{R}^i$ is the rotation matrix of each bar element i. In fact, this equilibrium equation is a consequence of the equality of all the spatial virtual displacements $\delta \boldsymbol{u}^{ij}$ of the bar ends connected to a joint j. Instead, the active virtual displacement δu_a^{ij} are internal and not shared among different bars.

3.3.2 Stress-dependent active displacements

In parallel with Eq. (22), we here hypothesise that the elastic and active bar displacements are related through a control function $C : \mathbb{R} \to \mathbb{R}$ as follows,

$$\dot{u}_a' = C(u_e'). \tag{34}$$

By inserting this evolution law into equations (23), noting that γ_a is equivalent to J_a and that $\dot{\gamma}_a = \dot{u}_a' = C$, we arrive at the following two relations,

$$\Gamma = \frac{\dot{u}_a'}{\gamma_a} = \frac{C}{\gamma_a}, \quad \left(\gamma_e q_e - \rho^0 \left(\psi + \frac{\partial \psi}{\partial \gamma_a}\gamma_a\right)\right) C' \gamma_a^{-1} - \Theta \bar{S} \geq 0, \tag{35}$$

where $C' = \frac{\partial}{\partial u_e'} C$, and here and in the following expressions, the argument of function C is omitted. We discretise in time Eq. (34) using the following Crank–Nicholson time-step algorithm:

$$u_{a,n+1}' = u_{a,n}' + \Delta t C_{n+\theta},$$

with $C_{n+\theta} = C(u_{e,n+\theta}')$. After noting $\delta u_a' = \gamma_e \delta u_a' + \gamma_a \delta u_e'$, the following relation between the virtual displacements is obtained:

$$\delta u_a' = \theta \Delta t C' (\delta u' - \gamma_{e,n+1} \delta u_a') \gamma_{a,n+1}^{-1}$$

or, rearranging terms,

$$\delta u_a' = \frac{\theta \Delta t C'}{\gamma_{a,n+1} + \theta \Delta t C' \gamma_{e,n+1}} \delta u'. \tag{36}$$

From these expressions, the minimisation of Π yields equivalent equations to those in (26):

$$\frac{\partial}{\partial X_1}\left(q_e + \left(\rho^0 \frac{\partial \psi}{\partial \gamma_a}\gamma_a + \rho^0 \psi - \gamma_e q_e\right) \times \frac{\gamma_a \theta \Delta t C'}{\gamma_a + \gamma_e \theta \Delta t C'}\right) = 0, \quad \forall X_1 \in [0, L] \tag{37}$$

3.3.3 Model simplifications

With the aim of applying our model to a biomechanical process, we particularise and simplify in this section those variables that are as yet undefined, namely the free energy function ψ and the control function C. The latter is now reduced to the following linear relationship:

$$\dot{u}_a' = \beta(q_e - q_T) = \beta(\rho^0 k u_e' - q_T), \tag{38}$$

where q_T is the *target stress*, assumed constant, and $\beta \geq 0$ is a material parameter. The physical interpretation of this law is simple: when $q_e > q_T$, that is, the bar is under tension, the bar elongates in order to diminish the actual elastic stress and vice-versa. The rate of active elongation or contraction is determined by the parameter β. Such a law is represented in Fig. 4. It is worth pointing out that if this law was applied to

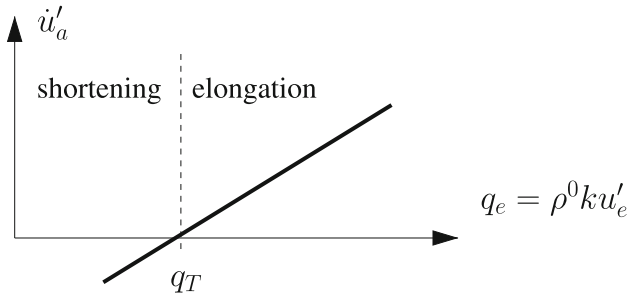

Fig. 4 Evolution law for the active deformations

a material that surrounds a cell, the limit value of the stresses q_T is equivalent to the behaviour of the membrane, which has a tendency to be at a constant stress state or surface tension q_T. A model that reproduces such constant stress state of the cell boundary is described in Brodland et al. (2006).

Due to the linearity of the evolution law in (38), we have that $C' = \beta\rho^0 k$, which is constant. Consequently, by resorting to Eq. (36), the following relations between $\delta u'$, δu_a and δu_e may be derived (see Appendix C):

$$\begin{aligned} \delta u'_a &= G\delta u' \\ \delta u'_e &= \frac{G}{\tau}\delta u'. \end{aligned} \tag{39}$$

where G and τ are defined also in Appendix C.

We additionally assume for simplicity that the free energy function does not depend on u_a, but solely on u_e. Furthermore, we choose an energy function that mimics the behaviour of a spring, that is we consider the following energy function ψ:

$$\psi = \frac{1}{2}k(tr(\boldsymbol{F}_e) - 3)^2 = \frac{1}{2}k(u'_e)^2 \tag{40}$$

with k a constant material parameter. We note that the elastic deformation of the bars is not assumed incompressible, since a variation of the cross-section area of the microfilament as it deforms would be unrealistic. Also, we point out that, although the stored energy in the *intermediate* configuration $\psi = J_a^{-1}\psi^0$ depends solely on $\boldsymbol{F}_e$, the free energy ψ^0 still depends on the two deformation gradients, $\boldsymbol{F}_a$ and $\boldsymbol{F}_e$. In this case, the stored energy ψ^0 increases even if $\boldsymbol{F}_e$ is constant due to the increase of matter when growth occurs. However, since ψ does not depend on $\boldsymbol{F}_a$, the configuration Ω is indeed stress-free, like in Rodriguez et al. (1994).

Using these simplifications, since $C' = \beta\rho^0 k$, the equation in (37) turns into,

$$\frac{\partial}{\partial X_1}\left(ku'_e\right) - \underline{\frac{\partial}{\partial X_1}\left((u'_e + \frac{1}{2}(u'_e)^2)kG\gamma_a\right)} = 0, \quad \forall X_1 \in [0, L] \tag{41a}$$

$$\left(ku'_e - (u'_e + \frac{1}{2}(u'_e)^2)kG\right) = \bar{\boldsymbol{q}} \cdot \boldsymbol{E}_1, \quad X_1 = \{0, L\}, \tag{41b}$$

where henceforth we omit the subscript $n+1$ for clarity. The local equation in (41a) differs substantially from the usual spatial equilibrium for bars, that is,

$$ku''_e = 0. \tag{42}$$

After comparing this equation and (41), it can be concluded that the active elongation process, together with the evolution law in (38), are equivalent to an additional body force given by the expression underlined in (41a). We remark that this additional body force is similar to considering additional material stresses, as the accretive forces introduced in DiCarlo and Quiligotti (2002), Ambrosi and Guana (2007). In our case, the additional terms in Eq. (41a) are a by-product of the coupling between the active and elastic deformations, which in turn couples the elastic equilibrium and the condition for growth in (33a).

By noting that the quadratic free energy function in (40) may be expressed as $\rho^0\psi = \frac{1}{2}q_e u'_e$, the reduced dissipation inequality in (35) simplifies to,

$$\left(1 + \frac{1}{2}u'_e\right)k\beta\Delta t\theta u'_e - \Theta\bar{S} \geq 0. \tag{43}$$

Since $\Theta > 0$, this equation allows to bound explicitly the entropy source as,

$$\bar{S} \leq \left(1 + \frac{1}{2}u'_e\right)k\beta\Delta t\theta u'_e\Theta^{-1}. \tag{44}$$

Moreover, since $\rho^0 > 0$, $C' = \beta\Delta t\,\theta > 0$ (for $\theta > 0$ and $\beta > 0$) and $\Delta t > 0$, it can be deduced that no extra entropy energy is strictly necessary when $u'_e > 0$. However, when $u'_e < 0$, the term $\bar{S}$ becomes necessary in order to satisfy the second law of thermodynamics. We note though that other more sophisticated forms of ψ and control functions C may allow to make $\bar{S}$ unnecessary in a larger set of situations. It is worth emphasising that although no microstructure has been explicitly considered, the fact that $\bar{S}$ becomes necessary when $u'_e < 0$ is physically in agreement with the fact that additional entropy is inserted in the system whenever the chain complex is in compression, that is, when the chain has more freedom to vibrate and therefore its entropy increases (a larger set of states are accessible for the given stored energy).

3.4 Finite element implementation

The equilibrium equations in (41) are solved at each time t by resorting to the finite element method. We therefore multiply the local equation in (41a) along direction $\boldsymbol{e}_1$ for each bar i by a test function (or virtual displacement) $\boldsymbol{w} = w\boldsymbol{e}_1$ and integrate over the domain of each bar, which yields

$$\int_L \boldsymbol{w}\cdot\boldsymbol{e}_1\frac{\partial}{\partial X_1}\left(u'_e - \left(1 + \frac{u'_e}{2}\right)u'_e G\gamma_a\right)k\,dL = 0,$$
$$\forall w \in \mathcal{H}^1,$$

where $\mathcal{H}^1$ is the Hilbert space of functions w whose L_2 norm, and the L_2 norm of the first derivatives are bounded. Due to the use of a Newton–Raphson iterative procedure, which requires the linearisation of the resulting equations, it is convenient to modify the previous expression as an integral along the reference length L^0. After integrating by parts, by making use of (41b) and using the finite element interpolation $\boldsymbol{w} \approx \boldsymbol{w}_i N_i(X_1^0)$, with $N_i(X_1^0)$ a set of complete functions, and w_i the set of arbitrary nodal values of the test functions $\boldsymbol{w}(\boldsymbol{X}_1^0)$, we obtain the following system of nonlinear equations:

$$\boldsymbol{g} = \bar{\boldsymbol{g}}. \tag{45a}$$

The component i, associated to node i in the vectors $\boldsymbol{g}$ and $\bar{\boldsymbol{g}}$ are, respectively, given by,

$$\boldsymbol{g}_i = \int_{L^0} N_i' \left(1 - \left(1 + \frac{u_e'}{2}\right) G\gamma_a\right) u_e' k \boldsymbol{e}_1 \, dL^0$$
$$\bar{\boldsymbol{g}}_i = \bar{\boldsymbol{q}}. \tag{45b}$$

It is shown in Appendix D that using linear interpolating functions $N_i(X_1^0)$ for the test functions and the deformed positions $\boldsymbol{x}(X_1^0) = N_i(X_1^0)\boldsymbol{x}^i$, the computation of the residual and its linearisation simplifies substantially.

4 Results

We will first analyse in a single cell the effects of the equilibrium conditions of the coupling active and passive deformations. The model is then used to simulate the invagination process in the *Drosophila melanogaster* embryo.

4.1 Single cell model

In order to quantify the differences between the equilibrium equations derived here and the standard elastic equations, we will here consider the simple truss model depicted in Fig. 5, formed by 4 nodes and 6 bars. All the bars are purely passive elastic ($\beta = 0$), except the horizontal bar at the bottom, which has the target stress $q_T = 0.25$. All the 6 bars have a stiffness parameter $k = 2$.

The inner volume of the cell is kept constant during the analysis. Due to the constraints applied to the nodes, the bottom bar tries to shorten in order to achieve the tensile target stress q_T. The model has been run solving the equilibrium equations after introducing the coupling (Eq. (45) and the standard elasticity equations in (42) in conjunction with the evolution law in (34). Figures 6a–b show the intermediate length L and the elastic deformation u_e' of the bottom bar, respectively. While the two set of equations yield obviously the same final homeostatic value of u_e', some difference

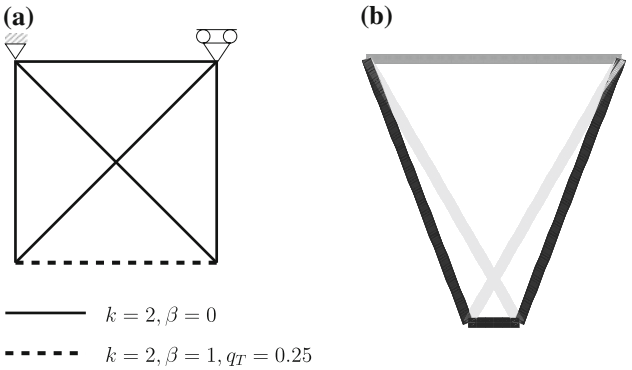

Fig. 5 Schematic model for one cell (**a**) and final deformation (**b**). *Dark and light grey* indicate tensile and compressive stresses, respectively

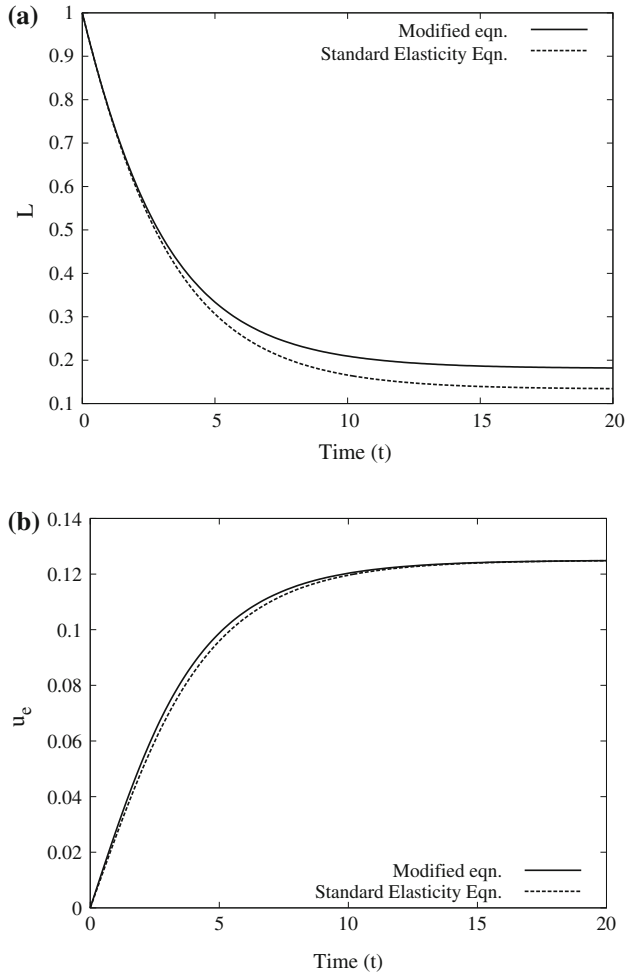

Fig. 6 Evolution of the active length L (**a**) and the elastic force (**b**) u_e' using the current approach and the standard elasticity equations

in their evolution can be appreciated. More importantly, the intermediate length L converges in each case to slightly different values, due to the presence of the additional underlined term in Eq. (41a).

4.2 Invagination of the *Drosophila melanogaster* embryo

We apply the truss model described so far to analyse the ventral furrow invagination in the *Drosophila melanogaster*. This process involves the first large deformations of the embryo and is characterised by the internalisation of the ventral cells into a furrow formation (see detailed description in (Costa et al. 1993)). The process is thought to be driven by shape changes caused by active structural changes in the cytoskeleton of individual epithelial cells surrounding the embryo.

4.2.1 Model geometry

As in previous work (Muñoz et al. 2007, 2009), we use a model of the embryo that consists of a 2D circular rigid membrane encapsulating an epithelium of single cell thickness, which itself surrounds a circular yolk. The epithelium of the embryo is discretised into 96 cells, 16 in the mesoderm (dark grey in Fig. 7) and 80 ectodermal cells (light grey). Each cell is composed by a set of basal (in contact with the yolk), apical (in contact with the membrane), lateral and internal bars, as depicted in Fig. 8. The external bars simulate the stiffness of the actin microfilament networks branching underneath the cellular membrane and the microtubules running through the cell from the apical to the basal side, whereas the internal bars simulate the rigidity furnished by the system, constituted by the cytoplasm, the nucleus and endoplasmic reticulum. The difference between cells in mesoderm and the ectoderm lies not only in their location in the embryo but also in their material properties, which will be described in the next section. The vitelline membrane that surrounds the embryo is assumed to be rigid. A unilateral contact condition is introduced between the epithelium and this external rigid material.

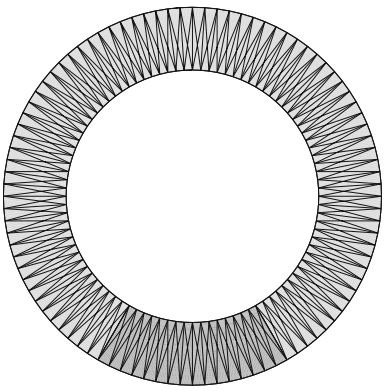

Fig. 7 Initial geometry and discretisation of the embryo cross-section. Ectoderm is in *light grey* and mesoderm in *dark grey*

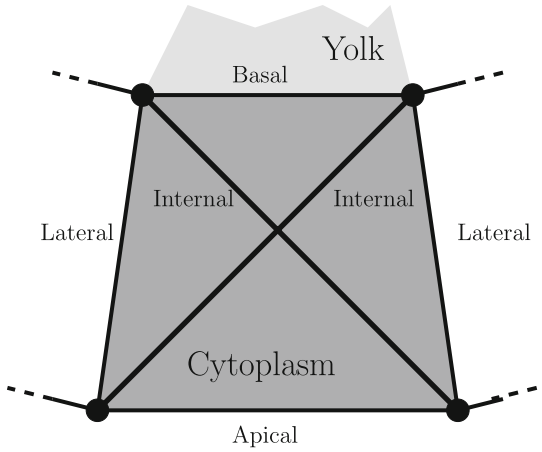

Fig. 8 Scheme of the trusses in the cells of the epithelium

4.2.2 Material parameters

The material stiffness k, density ρ^0, target stress q_T and material parameter β employed for the different bar elements of the embryo are given in Table 2. Ectoderm and mesoderm have the same stiffness properties. External bar elements (basal, apical and lateral, see Fig. 8) have the same value of $k = 50$, while the one of the internal cells is 4 times larger.

Superimposed onto the deformation of the cytoskeleton, it is assumed that the yolk and the cell cytoplasm are inviscid nearly incompressible materials. We model them by just imposing the incompressibility of each cell and the whole yolk. This is equivalent to supplementing the free energy density with the following term:

$$\psi_{inc} = \frac{p_y}{2}\left(v_y - V_y^0\right)^2 + \frac{p_c}{2}\sum_{i=1}^{nel}\left(v_{c,i} - V_{c,i}^0\right)^2$$

where p_c and p_y are penalty parameters, V_y^0 and v_y are the initial and deformed volume of the yolk and $V_{c,i}^0$ and $v_{c,i}$ are the initial and deformed volume of the quadrilateral element i. We note that each cell in the model represents one

Table 2 Material and time-integration parameters

Epithelium	Cytoskeleton	k	ρ^0	q_T	β
Ectoderm	Apical	50	1	0	0
Ectoderm	Basal	50	1	0	0
Ectoderm	Lateral	50	1	0.03	10
Ectoderm	Internal	200	1	0.03	10
Mesoderm	Apical	50	1	0.03	50
Mesoderm	Basal	50	1	0	0
Mesoderm	Lateral	50	1	0	0
Mesoderm	Internal	200	1	0	0

biological cell, and therefore, the incompressibility of the former is a necessary but not sufficient condition for the pointwise volume preservation of the fluid in the cell. We assume that this discrepancy does not affect exceedingly our final deformations. The higher the values of the penalty parameters p_c and p_y are, the more accurate the incompressibility constraints $v_y - V_y^0 = 0$ and $v_{i,c} - V_{i,c}^0 = 0$ are, but also the more ill-conditioned the system of equations becomes. We have chosen the values $p_c = 6$ and $p_y = 0.05$, which is a compromise between accuracy and solvability of the numerical simulations. In all cases, we obtained volume differences smaller than 4%.

The parameters employed for the control function are listed in Table 2. We have simulated the apical constriction of the mesodermal cells (shortening of their apical side, see Fig. 8) by assigning the values $\beta = 0.03$ and $q_T = 50$ to the apical bars in the mesoderm. A radial thinning of the ectodermal domain is introduced by assigning is simulated assigning also the values $\beta = 0.03$ and $q_T = 10$ to the lateral and internal cells. These parameters intend to provide reference values in order to represent the qualitative behaviour of the cells.

The nonlinear differential equations have been integrated by using the parameter $\theta = 0.5$ and a time-step size $\Delta t = 0.05$, which has been able to solve the nonlinear equations without convergence problems. For the values of k and β employed, the duration of the invagination process is found to be approximately 0.9 time units.

4.2.3 Influence of boundary constraints

Figure 9a shows that with all the constraints activated (vitelline membrane contact conditions and incompressibility of the cell cytoplasm and the yolk) the stress feedback mechanism can reproduce successfully ventral invagination. This is an important result since it shows that even though each cell behaves in an autonomous manner, changing shape to satisfy its own internal stress-state requirements, a coordinated global morphogenetic movement is accomplished. In other words, invagination of an embryo can be brought about through stress control alone, without the need for other regulatory or signalling mechanisms.

In order to investigate the main mechanism responsible of the invagination process, we have tested the same model but in the absence of some of the constraints. Interestingly, we found that when the yolk is removed, the ventral cells do not invaginate. Figure 9b shows the deformed configuration at the same time $t = 0.85$ as for the successful invagination, and with the same stress limits, but with the yolk missing. We have also shown in the same figure the elastic stress of the bars. Dark grey is a positive (tensile) stress, while lighter grey corresponds to negative (compressive) stress. Comparison of the stress profiles in Fig. 9 indicates that the apical bars

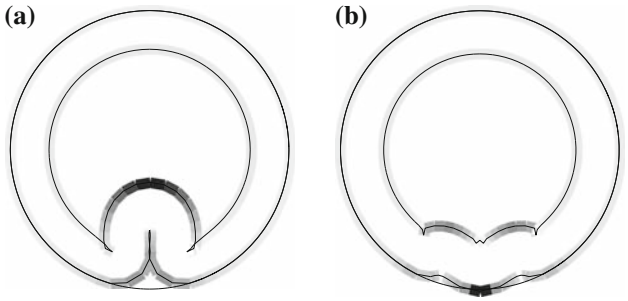

Fig. 9 Stress intensity of the external bars of the cross-section with the yolk constraint (**a**) and without it (**b**). *Dark grey* are positive stresses (tension) and *light grey* are negative stresses (compression)

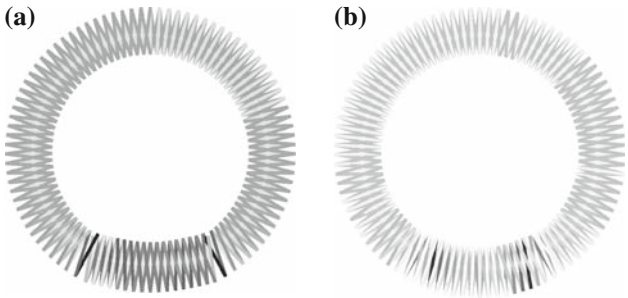

Fig. 10 Stress profile at the internal and lateral *bars* applying the yolk constraint (**a**) and removing it (**b**). *Darker grey* means larger tensile stresses

shorten, but while this shortening is favoured in successful invagination, in the failed invagination the apical bars remain under tension. The incompressibility constraint of the yolk produces a negative pressure due to the shortening of the ectoderm. This negative pressure is apparently necessary to rise the mesoderm. The stress profile of the internal and lateral bars in Fig. 10 at $t = 0.3$, reveals that indeed, in the presence of the yolk, these bars are in general under a higher tensile stress. Eventually, at $t = 0.5$, the mesoderm has successfully risen, while in the absence of the yolk constraint, the mesoderm remains at the bottom of the ventral side (see Fig. 9). Figure 11 shows the profile of the deformed epithelium at this instant. Interestingly, similar deformed configurations are achieved if we increase the β-values of the apical mesodermal bars and we leave those of all the ectodermal bars unaltered, i.e. if we favour apical constriction of mesodermal cells (mesodermal arching) against radial shortening of ectodermal cells (ectodermal pushing).

5 Conclusions

A set of equilibrium equations has been derived for the stress-controlled shape change of cells due to the remodelling and growth of their internal architecture. The approach involves

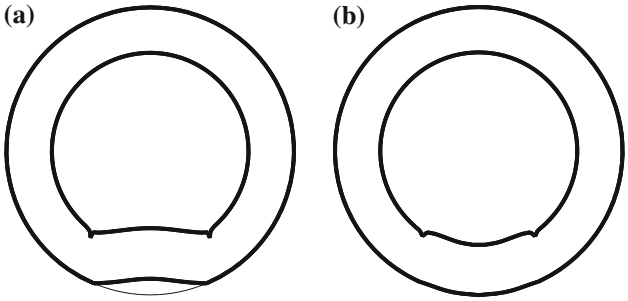

Fig. 11 Profile of the deformed configuration of the cross-section with the yolk constraint (*a*) and without it (*b*)

the decomposition of the deformation gradient into an active and a passive component, where the former is allowed to include a growth process, while the latter is assumed to be hyperelastic and mass-preserving. The two components are coupled with a control function that provides the required feedback mechanism. While such a control law has already been introduced in Rodriguez et al. (1994), Taber (2008), Ramasubramanian and Taber (2008), the resulting modified equilibrium equations, and their particularisation to a truss system, have not to our knowledge been previously studied.

The results are applied to a system of trusses whose function is to simulate the cytoskeletal network constituted by myosin microfilaments and microtubules, which are found experimentally to control shape change in cells. The behaviour of the system is justified by a thermodynamically consistent arguments stemming from a continuum model.

The model has been used to simulate the multicellular shape changes observed during ventral furrow invagination of the *Drosophila melanogaster* embryo. The results show that ventral furrow invagination can be achieved through stress control alone, without the need for other regulatory or signalling mechanisms. The model also reveals that the yolk plays a distinct role in the process: the presence of the inner incompressible yolk alters the mesodermal stress configuration so as to contribute to the formation of the ventral furrow by facilitating its inward bending and rise. This feature emerges in the system because active deformations are determined through stress-controlled feedback mechanisms, which provides the necessary active response. It is interesting to notice that our previous models (Muñoz et al. 2007; Conte et al. 2008) were not able to reproduce this feature because active deformations were externally imposed independently from the inner stress state of the material. Accordingly, in these works, the alterations in the mesodermal stress induced by the inner yolk were uncoupled from the imposed active deformations and, therefore, did not affect epithelial phenotype.

As a consequence, the results shown here are an important contribution to the study of self-assembling living organisms, in that they provide further evidence that stress can play an important role (as also recently shown in Ramasubramanian and Taber 2008, Taber 2008) and they give further evidence in favour of Beloussov's hyper-restoration hypotheses.

We have here restrained our model to constant target stresses. Variable target stresses have been modelled and implemented in Taber (2008), which may be a more realistic assumption. However, we note that the correct choice of a variable or constant target stress requires first the determination of the cellular parameters that determine the active response of the cytoskeleton, and also further experimental analysis to elucidate how these parameters vary.

A Derivation of the constraints due to the control function

From the general time-stepping in (24), we obtain the following relationship between the virtual active displacements $\delta \boldsymbol{u}_a$ and $\delta \boldsymbol{u}_e$:

$$\delta \boldsymbol{F}_a = \theta \Delta t \nabla \boldsymbol{C}_{n+\theta} : \left((\delta \boldsymbol{F}) \boldsymbol{F}_a^{-1} - \boldsymbol{F}_e (\delta \boldsymbol{F}_a) \boldsymbol{F}_a^{-1} \right),$$

where $[\nabla \boldsymbol{C}]_{ijkl} = \frac{\partial [C]_{ij}}{\partial [F_e]_{kl}}$. This relation may be written as,

$$\delta \boldsymbol{F}_a = (\boldsymbol{\mathcal{I}} + \boldsymbol{F}_e^{\mathrm{T}} \boldsymbol{\mathcal{K}})^{-1} \boldsymbol{\mathcal{K}} : \delta \boldsymbol{F} = \boldsymbol{\mathcal{L}} : \delta \boldsymbol{F},$$

whenever the fourth-order tensor $(\boldsymbol{\mathcal{I}} + \boldsymbol{F}_e^{\mathrm{T}} \boldsymbol{\mathcal{K}})$ is invertible. $\mathcal{I}_{ijkl} = \delta_{ij} \delta_{kl}$ is the fourth-order identity tensor, and $\boldsymbol{\mathcal{K}} = \theta \Delta t (\nabla \boldsymbol{C}) \boldsymbol{F}_a^{-\mathrm{T}}$ is given, in indicial notation, as $[\mathcal{K}]_{ijkl} = [\nabla C]_{ijkm} [F_a^{-1}]_{lm}$, whereas the product $\boldsymbol{F}_e^{\mathrm{T}} \boldsymbol{\mathcal{K}}$ denotes $[\boldsymbol{F}_e^{\mathrm{T}} \boldsymbol{\mathcal{K}}]_{ijkl} = [F_e]_{mk} [\nabla \boldsymbol{C}]_{ijml}$.

B Strain and stress measures for bars

Let us express the associated first Piola–Kirchhoff stress as $\boldsymbol{P} = \boldsymbol{P}_i \otimes \boldsymbol{E}_i$, where $\boldsymbol{P}_i = P_i \boldsymbol{e}_i$ (no summation on i) is the tension in the deformed configuration per unit area perpendicular to the $\boldsymbol{E}_i$ direction in the reference configuration. The time differentiation of the deformation gradient $\boldsymbol{F}$ is, according to relations in (27), equal to,

$$\dot{\boldsymbol{F}} = \hat{\boldsymbol{\omega}} \boldsymbol{e}_i \otimes \boldsymbol{E}_i + \dot{u}' \boldsymbol{e}_1 \otimes \boldsymbol{E}_1 + u' \hat{\boldsymbol{\omega}} \boldsymbol{e}_1 \otimes \boldsymbol{E}_1 \tag{46}$$

where $\boldsymbol{\omega}^{\mathrm{T}} = (\omega_1, \omega_2, \omega_3)$ is the angular velocity and the symbol $\hat{\boldsymbol{\omega}}$ denotes the skew-symmetric matrix $\hat{\boldsymbol{\omega}} = \begin{bmatrix} 0 & -\omega_3 & \omega 2 \\ \omega_3 & 0 & -\omega_1 \\ -\omega_2 & \omega_1 & 0 \end{bmatrix}$, such that $\hat{\boldsymbol{u}} \boldsymbol{v} = -\hat{\boldsymbol{v}} \boldsymbol{u} = \boldsymbol{u} \times \boldsymbol{v}$. With this notation, and the expression in (46), the tensor product $\boldsymbol{P} : \dot{\boldsymbol{F}}$ results in,

$$\begin{aligned} \boldsymbol{P} : \dot{\boldsymbol{F}} &= -\mathrm{tr}((\boldsymbol{P}_i \otimes \boldsymbol{e}_i) \hat{\boldsymbol{\omega}}) - u' \mathrm{tr}((\boldsymbol{P}_1 \otimes \boldsymbol{e}_1) \hat{\boldsymbol{\omega}}) + \dot{u}' \boldsymbol{P}_1 \cdot \boldsymbol{e}_1 \\ &= -\boldsymbol{\omega} \cdot (\hat{\boldsymbol{P}}_i \boldsymbol{e}_i + u' \hat{\boldsymbol{P}}_1 \boldsymbol{e}_1) + \dot{u}' \boldsymbol{P}_1 \cdot \boldsymbol{e}_1. \end{aligned} \tag{47}$$

To proceed further, we note that the ij component of $\boldsymbol{P}\boldsymbol{F}^{\mathrm{T}} - \boldsymbol{F}\boldsymbol{P}^{\mathrm{T}}$ is given by,

$$[\boldsymbol{P}\boldsymbol{F}^{\mathrm{T}} - \boldsymbol{F}\boldsymbol{P}^{\mathrm{T}}]_{ij} = \sum_k \left([\boldsymbol{P}_k]_i \frac{\partial x_j}{\partial X_k} - \frac{\partial x_i}{\partial X_k} [\boldsymbol{P}_k]_j \right) = \sum_k \epsilon_{ijl} \left[\hat{\boldsymbol{P}}_k \frac{\partial \boldsymbol{x}}{\partial X_k} \right]_l$$

with ϵ_{ijl} the permutation index. Since $\boldsymbol{P}\boldsymbol{F}^{\mathrm{T}} - \boldsymbol{F}\boldsymbol{P}^{\mathrm{T}} = \boldsymbol{0}$, it follows that $\sum_k \hat{\boldsymbol{P}}_k \frac{\partial \boldsymbol{x}}{\partial X_k} = \boldsymbol{0}$, which for the kinematics of the bar described here yields,

$$\hat{\boldsymbol{P}}_i \boldsymbol{e}_i + u' \hat{\boldsymbol{P}}_1 \boldsymbol{e}_1 = \boldsymbol{0}.$$

Using this relation in Eq. (47) and denoting by $\boldsymbol{q}_q = \int_{A^0} \boldsymbol{P}_1 dA^0$, we have that the stress power $\dot{W} = \int_{V^0} \boldsymbol{P} : \dot{\boldsymbol{F}}\, dV^0$ reduces to,

$$\dot{W} = \int_{L^0} \dot{u}' \boldsymbol{e}_1 \cdot \boldsymbol{q}_q \, \mathrm{d}X_1^0 = \int_{L^0} \dot{u}' \boldsymbol{E}_1 \cdot \boldsymbol{q} \, \mathrm{d}X_1^0,$$

where $\boldsymbol{q} = \boldsymbol{R}^{\mathrm{T}} \boldsymbol{q}_q$, with $\boldsymbol{R}$ the rotation matrix introduced in Sect. 3.1. Since $u'\big|_{t=0} = 0$, it follows from this equation that we can then define $\boldsymbol{\varepsilon} = (1 + u')\boldsymbol{E}_1$ as the strain measure of the bars, conjugate to the stress measure $\boldsymbol{q}_e$, and then rewrite the stress power as:

$$\dot{W} = \int_{L^0} \dot{\boldsymbol{\varepsilon}} \cdot \boldsymbol{q} \, \mathrm{d}X_1^0 = \int_L (1 + u'_a)^{-1} \dot{\boldsymbol{\varepsilon}} \cdot \boldsymbol{q} \, \mathrm{d}X_1, \tag{48}$$

where, after assuming $u'_a + 1 > 0$, we have made use of the identity $\mathrm{d}X_1 = |1 + u'_a| \, \mathrm{d}X_1^0 = (1 + u'_a) \, \mathrm{d}X_1$.

C Relation between virtual displacements in bars

By introducing the following definitions:

$$\tau = \theta \Delta t \beta \rho^0 k \tag{49}$$

$$G = \frac{\tau}{\gamma_{a,n+1} + \tau \gamma_{e,n+1}}, \tag{50}$$

the relations between $\delta u'_a$ and $\delta u'$ in (36), and $\delta u'_e$ and $\delta u'$, read

$$\delta u'_a = G \delta u'$$

$$\delta u'_e = (\delta u' - \gamma_e \delta u'_a) \gamma_a^{-1} = \frac{G}{\tau} \delta u'.$$

We emphasise that G may be expressed solely as a function of the elastic displacement, since the active displacement may be related to u_e through the evolution law in (38). By resorting to the previous relations, the variation of $G(u'_e)$ is obtained as,

$$\delta G = -\frac{G^2}{\tau}(\tau \delta u'_e + \delta u'_a) = -\frac{2G^3}{\tau} \delta u'. \tag{51}$$

D Residual vector and Jacobian of the equilibrium equations

If the deformed positions are interpolated as $\boldsymbol{x}(X_1^0) = N_i(X_1^0)\boldsymbol{x}^i$, with $N_i(X_1^0)$ a set of complete linear functions, the vectors u' and $\delta u'$ are element-wise constant and equal to:

$$1 + u' = \boldsymbol{x}' \cdot \boldsymbol{e}_1 = \frac{\boldsymbol{x}^2 - \boldsymbol{x}^1}{L^0} \cdot \boldsymbol{e}_1 = \frac{\ell \boldsymbol{e}_1}{L^0} \cdot \boldsymbol{e}_1 = \frac{\ell}{L^0},$$

$$\delta u' \boldsymbol{e}_1 = \frac{\delta \ell}{L^0} \boldsymbol{e}_1 = \boldsymbol{e}_1 \otimes \boldsymbol{e}_1 \delta \boldsymbol{x}' \tag{52}$$

where $\boldsymbol{x}^1$ and $\boldsymbol{x}^2$ are the nodal deformed positions. Furthermore, from this result, and the relationships in (29) and (38), the elastic and active deformations may be explicitly obtained as,

$$u'_e = \frac{-1 - c_n - \tau \pm \sqrt{(1 + c_n - \tau)^2 + \frac{4\ell\tau}{L^0}}}{2\tau}$$

$$u'_a = \frac{\ell}{L^0(1 + u'_e)} \tag{53}$$

where c_n does not depend on variables at the current time-step $n + 1$, and is given by,

$$c_n = u'_{a,n} + \Delta t \beta \left(\rho^0 k (1 - \theta) u'_{e,n} - q_T \right).$$

After observing the expressions of u'_e and u'_a in (53), it can be concluded that the linearity of $\boldsymbol{x}$ implies the linearity of u, u_e and u_a. Therefore, the intermediate length may be computed as,

$$L = (1 + u'_a) L^0 = \frac{\ell}{1 + u'_e}.$$

We remark that these equalities allow us to use ℓ and L as primary unknowns, instead of u'_e and u'_a, and rewrite ψ, γ_a and γ_e simply as,

$$\psi = \frac{1}{2} k \left(\frac{\ell - L}{L} \right)^2, \quad \gamma_a = \frac{L}{L^0}, \quad \gamma_e = \frac{\ell}{L}$$

The nonlinear system of equations in (45b) are solved by resorting to a Newton–Raphson iterative process, which requires the computation of the Jacobian matrix $\boldsymbol{K}$ of the residual vector $\boldsymbol{g}$ in (45). It can be verified that, using relations (39) and (51), the component K_{ij}, corresponding to the contribution of nodes i and j, is given by,

$$\boldsymbol{K}_{ij} = \int_{L^0} N'_i N'_j \, (c_1 + c_2) \, k \boldsymbol{e}_1 \otimes \boldsymbol{e}_1 \, \mathrm{d}L^0 + \int_{L^0} N'_i N'_j c_3 \frac{k L^0}{\ell} \boldsymbol{M} \, \mathrm{d}L^0$$

with $\boldsymbol{M} = \boldsymbol{I} - \boldsymbol{e}_1 \otimes \boldsymbol{e}_1$, and

$$c_0 = \left(1 + \frac{u_e'}{2}\right) u_e',$$
$$c_1 = (1 - \gamma_e G \gamma_a) \frac{G}{\tau},$$
$$c_2 = c_0 G^3 \left(\frac{\gamma_a}{\tau} - \gamma_e\right),$$
$$c_3 = u_e' - c_0 G \gamma_a.$$

Acknowledgments The authors would like to thank Antonio DiCarlo for his helpful discussions during the visit of the first author to Universita Roma Tre, Italy. This visit has been financed by the Spanish Minister of Science and Education through the research program 'Acciones Integradas', Ref. ACI20065650004071.

References

Ambrosi D, Guana F (2007) Stress-modulated growth. Math Mech Solids 12:319–342

Beloussov LV (1998) The dynamic architecture of a developing organism: an interdisciplinary approach to the development of organisms. Kluwer, Dordrecht

Beloussov LV, Saveliev SV, Naumidi II, Novoselov VV (1994) Mechanical stresses in embryonic tissues patterns morphogenetic, role and involvement in regulatory feedback. Int Rev Cytol 150: 1–34

Boyce MC, Arruda EM (2000) Constitutive models of rubber elasticity: constitutive models of rubber elasticity: a review. Rubber Chem Technol 73:504–523

Brodland GW, I-Li Chen D, Veldhuis JH (2006) A cell-based constitutive model for embryonic epithelia and other aggregates of biological cells. Int J Plast 22:965–995

Conte V, Muñoz JJ, Miodownik M (2008) 3D finite element model of ventral furrow invagination in the Drosophila melanogaster embryo. J Mech Behav Biomed Mater 2:188–198

Costa M, Sweeton D, Wieschaus E (1993) The development of drosophila melanogaster. chap 8: gastrulation in drosophila: cellular mechanisms of morphogenetic movements. Cold Spring Laboratory Press

DiCarlo A, Quiligotti S (2002) Growth and balance. Mech Res Commun 29:449–456

Epstein M, Maugin GA (2000) Thermomechanics of volumetric growth in thermomechanics of volumetric growth in uniform bodies. Int J Plast 16:951–978

Eshelby JD (1951) The force on an elastic singularity. Philos Trans R Soc Lond A 6:87–112

Garikipati K, Olberding JE, Narayanan H, Arruda EM, Grosh K, Calve S (2006) Biological remodelling: stationary energy, configurational change, variables and dissipation. J Mech Phys Solids 54:1493–1515, arXiv:q-bio/0506023v2

Gonzalez O, Stuart AM (2008) A first course in continuum mechanics. Cambridge University Press, Cambridge

Gurtin ME (2000) Configurational forces as basic concepts of continuum physics. vol 137 of Appl Math Sci. Springer

Himpel G, Kuhl E, Menzel A, Steinmann P (2005) Computational modelling of isotropic multiplicative growth. Comput Model Eng Sci 8:119–134

Holzapfel GA (2000) Nonlinear solid mechanics. A continuum approach for engineers. Wiley, New York

Humphrey JD (2001) Cardiovascular Solid Mechanics. Springer, Berlin

Ingber DE (1997) Tensegrity: the architectural basis of cellular mechanotransduction. Ann Rev Physiol 59:575–599

Kienzler R, Herrmann G (2000) Mechanics in material space. Springer, New York

Kuhl E, Steinmann P (2003) On spatial and material settings of thermo-hyperelastodynamics for open systems. Acta Mech 160:179–217

Kuhl E, Steinmann P (2004) Material forces in open systems mechanics. Comput Methods Appl Mech Eng 193:2357–2381

Kuhl E, Garikipati K, Arruda EM, Grosh K (2005) Remodeling of biological tissue: mechanically induced reorientation of a transversely isotropic chain network. J Mech Phys Solids 53:1552–1573

Kuhl E, Menzel A, Garikipati K (2006) On the convexity of transversely isotropic chain network models. Philos Mag 86:3241–3258

Lubarda VA, Hoger A (2002) On the mechanics of solids with a on the mechanics of solids with a growing mass. Int J Solids Struct 39:4627–4664

Lubarda VA (2004) Constitutive theories based on the multiplicative decomposition of deformation gradient: thermoelasticity, elastoplasticity, and biomechanics. Appl Mech Rev 57:95–108

Maugin GA (1995) Material forces: concepts and applications. Appl Mech Rev 48(5):213–245

Maugin GA, Berezovski A (2008) Introduction to the thermodynamics of configurational forces. Atti Accad. Pelorit. Peric LXXXVI(Supl. 1); doi:10.1478/C1S0801016

Miehe C, Göktepe S, Lulei F (2004) Progressive delamination using progressive delamination using interface elements. J Mech Phys Solids 52:2617–2660

Mizuno D, Tardin C, Schmidt CF, MacKintosh FC (2007) Nonequilibrium mechanics of active cytoskeletal networks. Science 315:370–373

Muñoz JJ, Barrett K, Miodownik M (2007) A deformation gradient decomposition method for the analysis of the morphogenesis. J Biomech, pp 1372–1380

Muñoz JJ, Conte V, Miodownik M (2009) Robust mechanisms of ventral furrow invagination require the shape changes. Phys Biol 6. doi:10.1088/1478-3975/6/1/016010

Odell GM, Oster G, Alberch P, Burnside B (1981) The mechanical basis of morphogenesis. I. Epithelial folding and invagination. Dev Biology 85:446–462

Rajagopal KR, Srinivasa AR (2004) On the thermomechanics of materials on the thermomechanics of materials that have multiple natural and classical plasticity. J Appl Math Phys (ZAMP) 55:861–893

Ramasubramanian A, Taber LA (2008) Computational modeling of morphogenesis regulated by mechanical feedback. Biomech Model Mechanobiol 7:77–91

Rodriguez EK, Hoger A, McCulloch AD (1994) Stress-dependent finite growth in soft elastic tissues. J Biomech 27:455–467

Simo JC (1985) A finite strain beam formulation. The three dimensional dynamic problem Part I. Comput Meth Appl Mech Eng 49:55–70

Stamenović D, Ingber DE (2009) Tensegrity-guided self assembly: tensegrity-guided self assembly: from molecules to living cells. Soft Matter 5(6):1137–1145

Steinmann P (2002) On spatial and material settings on spatial and material settings on thermo–hyperelastodynamics. J Elast 66: 109–157

Taber LA (1995) Biomechanics of growth, remodeling, and morphogenesis. Appl Mech Rev 48(8):487–545

Taber LA (1998) A model for aortic growth based on shear fibre stresses. J Biomech Eng 120:348–354

Taber LA (2008) Theoretical study of Beloussov's hyper-restoration hypothesis for mechanical regulation of morphogenesis. Biomech Model Mechanobiol. doi:10.1007/s10237-007-0106-x